Game Changing Development Program
Next Generation Life Support Project
Oxygen Recovery From Carbon Dioxide Using Ion
Exchange Membrane Electrolysis Technology—Final Report

Kenneth A. Burke
Glenn Research Center, Cleveland, Ohio

Feng Jiao
University of Delaware, Newark, Delaware

NASA STI Program . . . in Profile

Since its founding, NASA has been dedicated to the advancement of aeronautics and space science. The NASA Scientific and Technical Information (STI) Program plays a key part in helping NASA maintain this important role.

The NASA STI Program operates under the auspices of the Agency Chief Information Officer. It collects, organizes, provides for archiving, and disseminates NASA's STI. The NASA STI Program provides access to the NASA Technical Report Server—Registered (NTRS Reg) and NASA Technical Report Server—Public (NTRS) thus providing one of the largest collections of aeronautical and space science STI in the world. Results are published in both non-NASA channels and by NASA in the NASA STI Report Series, which includes the following report types:

- TECHNICAL PUBLICATION. Reports of completed research or a major significant phase of research that present the results of NASA programs and include extensive data or theoretical analysis. Includes compilations of significant scientific and technical data and information deemed to be of continuing reference value. NASA counter-part of peer-reviewed formal professional papers, but has less stringent limitations on manuscript length and extent of graphic presentations.

- TECHNICAL MEMORANDUM. Scientific and technical findings that are preliminary or of specialized interest, e.g., "quick-release" reports, working papers, and bibliographies that contain minimal annotation. Does not contain extensive analysis.

- CONTRACTOR REPORT. Scientific and technical findings by NASA-sponsored contractors and grantees.

- CONFERENCE PUBLICATION. Collected papers from scientific and technical conferences, symposia, seminars, or other meetings sponsored or co-sponsored by NASA.

- SPECIAL PUBLICATION. Scientific, technical, or historical information from NASA programs, projects, and missions, often concerned with subjects having substantial public interest.

- TECHNICAL TRANSLATION. English-language translations of foreign scientific and technical material pertinent to NASA's mission.

For more information about the NASA STI program, see the following:

- Access the NASA STI program home page at http://www.sti.nasa.gov

- E-mail your question to help@sti.nasa.gov

- Fax your question to the NASA STI Information Desk at 757-864-6500

- Telephone the NASA STI Information Desk at 757-864-9658

- Write to:
  NASA STI Program
  Mail Stop 148
  NASA Langley Research Center
  Hampton, VA 23681-2199
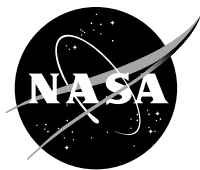
Game Changing Development Program
Next Generation Life Support Project
Oxygen Recovery From Carbon Dioxide Using Ion
Exchange Membrane Electrolysis Technology—Final Report

Kenneth A. Burke
Glenn Research Center, Cleveland, Ohio

Feng Jiao
University of Delaware, Newark, Delaware

Level of Review: This material has been technically reviewed by technical management.

Available from

Contents

List of Tables

List of Figures

Game Changing Development Program Next Generation Life Support Project
Oxygen Recovery From Carbon Dioxide Using Ion Exchange Membrane Electrolysis Technology—Final Report

Kenneth A. Burke
National Aeronautics and Space Administration
Glenn Research Center
Cleveland, Ohio 44135

Feng Jiao
University of Delaware
Newark, Delaware 19716

Executive Summary

This report summarizes the Phase I research and development work performed during the March 13, 2015 to July 13, 2016 period. The proposal for this work was submitted in response to NASA Research Announcement NNH14ZOA001N, "Space Technology Research, Development, Demonstration, and Infusion 2014 (SpaceTech-REDDI-2014)," Appendix 14GCD-C2 "Game Changing Development Program, Advanced Oxygen Recovery for Spacecraft Life Support Systems Appendix" The Task Agreement for this Phase I work is Document Control Number: GCDP-02-TA-15015.

The objective of the Phase I project was to demonstrate in laboratories two Engineering Development Units (EDU) that perform critical functions of the low temperature carbon dioxide electrolysis and the catalytic conversion of carbon monoxide into carbon and carbon dioxide. The low temperature carbon dioxide electrolysis EDU was built by the University of Delaware with Dr. Feng Jiao as the principal investigator in charge of this EDU development (under NASA Contract NNC15CA04C). The carbon monoxide catalytic conversion EDU was built by the NASA Glenn Research Center with Kenneth Burke as the principal investigator and overall project leader for the development of both EDUs. Both EDUs were successfully developed and demonstrated the critical functions for each process. The carbon dioxide electrolysis EDU was delivered to the NASA Johnson Space Center and the carbon monoxide catalytic conversion EDU was delivered to the NASA Marshall Spaceflight Center.

1.0   Introduction

The National Research Council's "NASA Space Technology Roadmaps and Priorities" identified long-duration environmental control and life support systems (ECLSS) as one of the top five areas capable of having the greatest impact on deep space exploration. The capability addressed represents an advanced system to further close the atmosphere revitalization loop on long duration human spacecraft. Space Technology Roadmap "Human Health, Life Support and Habitation Systems, Technology Area 06" calls for the atmosphere revitalization goal of 100 percent oxygen recovery by 2017. The problem was clearly identified in the NASA Research Announcement Appendix NNH14ZOA001N-14GCD-C2.

"NASA's previous human spaceflight studies have identified the development of advanced oxygen recovery systems as a key capability required for extending human presence throughout the solar system. Incomplete carbon dioxide reduction and oxygen recovery are considered major shortcomings for the current atmosphere revitalization systems…"

The proposed solution that was implemented is a two-step process that provides 100 percent oxygen capture and recycle. The first step is an ambient temperature carbon dioxide electrolyzer that converted carbon dioxide into carbon monoxide and oxygen. The carbon monoxide product of the electrolysis is fed into a catalytic bed reactor that produces elemental carbon and carbon dioxide which is recycled to the electrolysis process. The overall process diagram is shown in Figure 1 and the overall oxygen recovery mass flows are shown in Figure 2.
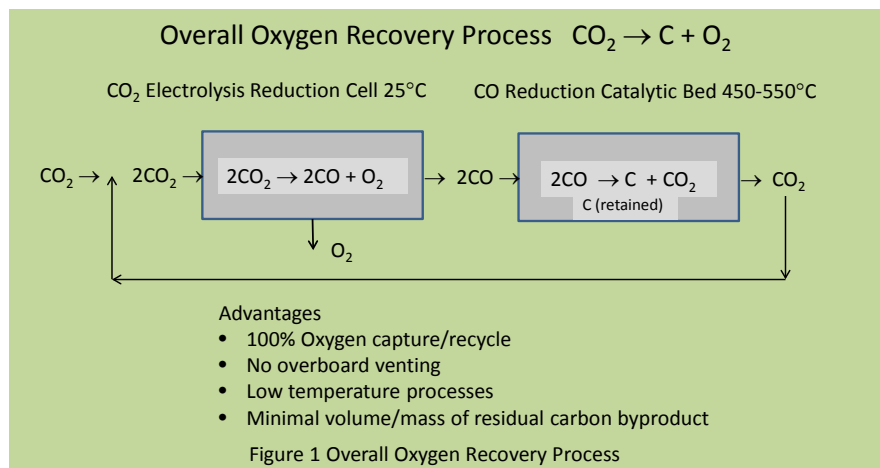
Figure 1.—Overall Oxygen Recovery Process.

Persons	1			2			3			4			5			6	
	g/day	g/hr	SLPM	g/day	g/hr	SLPM	g/day	g/hr	SLPM	g/day	g/hr	SLPM	g/day	g/hr	SLPM	g/day	g/hr
0.25	250	10.4	0.09	500	20.8	0.18	318	13.3	0.18	182	7.6	0.09	250	10.4	0.09	68	2.84
1	1000	41.7	0.35	2000	83.3	0.71	1273	53.0	0.71	727	30.3	0.35	1000	41.7	0.35	273	11.36
4	4000	166.7	1.42	8000	333.3	2.83	5091	212.1	2.83	2909	121.2	1.42	4000	166.7	1.42	1091	45.45
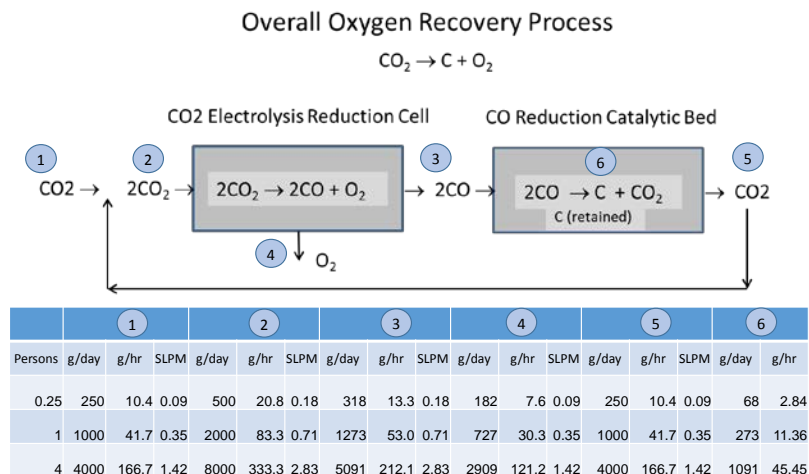
Figure 2.—Overall Oxygen Recovery Mass Flows.

The objective of the Phase I project was to demonstrate in laboratories two Engineering Development Units (EDU) that performed the critical functions and characteristics of the low temperature carbon dioxide electrolysis and the catalytic conversion of carbon monoxide into carbon and carbon dioxide. The Phase II project objective will be the integration of these two processes into a single oxygen recovery prototype system.

2.0   Carbon Dioxide Electrolysis

2.1   Single Cell

2.1.1   Design

Figure 3 shows the basic concept of CO_2 electrolysis flow cell using a polymer membrane. Based on the type of membrane (anion vs. cation exchange), the chemical reactions at the electrodes are summarized in Figure 3. In the design, a proton exchange membrane was selected for the single cell. Nanoporous Ag is the cathode material and IrO_2 is the anode material.

2.1.2   25 cm^2 Single CO_2 Electrolysis Flow Cell Fabrication

CO_2 Electrolyzer Cell∗

Cathode	Anode

Anion Exchange Membrane
Reaction $2CO_2 + 2H_2O + 4e^- \rightarrow 2CO + 4OH^-$
Theoretical Voltage vs RHE   −0.94 V

Anion Exchange Membrane
Reaction $4OH^- \rightarrow O_2 + 2 H_2O + 4e^-$
Theoretical Voltage vs RHE   +0.401 V

Cation Exchange Membrane
Reaction $2CO_2 + 4H^+ + 4e^- \rightarrow 2CO + 2H_2O$
Theoretical Voltage vs RHE   −0.11 V

Cation Exchange Membrane
Reaction $2H_2O \rightarrow O_2 + 4H^+ + 4e^-$
Theoretical Voltage vs RHE   +1.229 V

np - Ag   Pt (others)

Overall Reaction $2CO_2 \rightarrow 2CO + O_2$

Advantages: ambient temperature, neutral pH process, quick/easy start-up & shutdown

∗ [1] Feng Jiao, et al, Nature Communications "A Selective and Efficient Electrocatalyst for Carbon Dioxide Reduction" 30 January 2014

Figure 3.—Membrane Based CO_2 Electrolysis Cell.

2.1.2.1   Nanoporous Ag Cathode

Nanoporous Ag cathodes were fabricated using a modified dealloying technique, which is known to be an effective method to fabricate nanoporous metals. The $40 \times 5 \times 5$ cm^3 Ag-Al ingot was purchased from Sophisticated Alloys, Ltd (USA) and was synthesized using a vacuum induction process. This ingot was then cut in to 25 cm^2 Ag-Al precursor sheets with thickness of 500 μm using electrical discharge machining. The precursor sheets were annealed at 546 °C for 24 hr and then quenched to achieve the desired solid solution phase. Subsequently, the precursor sheets were leached in 1000 mL of 5 wt% HCl for 1 hr, rinsed several times in de-ionized water, and then dried in a vacuum oven overnight. The as-fabricated 25 cm^2 nanoporous Ag cathode electrode and a SEM image of the Ag electrode can be seen in Figure 4(a) and (b). Figure 4(c) and (d) show the Nafion XL membrane with Ir particles coated on anode side of the membrane and a typical SEM image of the Ir catalysis coated on the Nafion.

2.1.2.2   Ir-Coated Nafion Membrane

Ir-based catalyst coated membrane anodes were constructed via a hand-airbrush technique. A catalyst ink was prepared by sonicating a slurry containing commercial iridium black nanoparticles (surface area 55 to 65 m^2 per gram, Premetek Co.), Nafion solution (5 wt%, DuPont), DI water, and isopropanol. The weight ratio of catalyst to dry Nafion ionomer was 4:1. The iridium containing slurry was then sprayed on to Nafion 211 that has been sandwiched between two self-adhesive Mylar laminate (DuPont) with a 25 cm^2 window. The resulting Ir-CCM anodes were dried at 40 °C for 1 hr. The procedure was repeated until a catalyst loading of 1 mg cm^{-2} was achieved.

The as-fabricated Ir-coated Nafion membrane and its structural information can be seen in Figure 4.
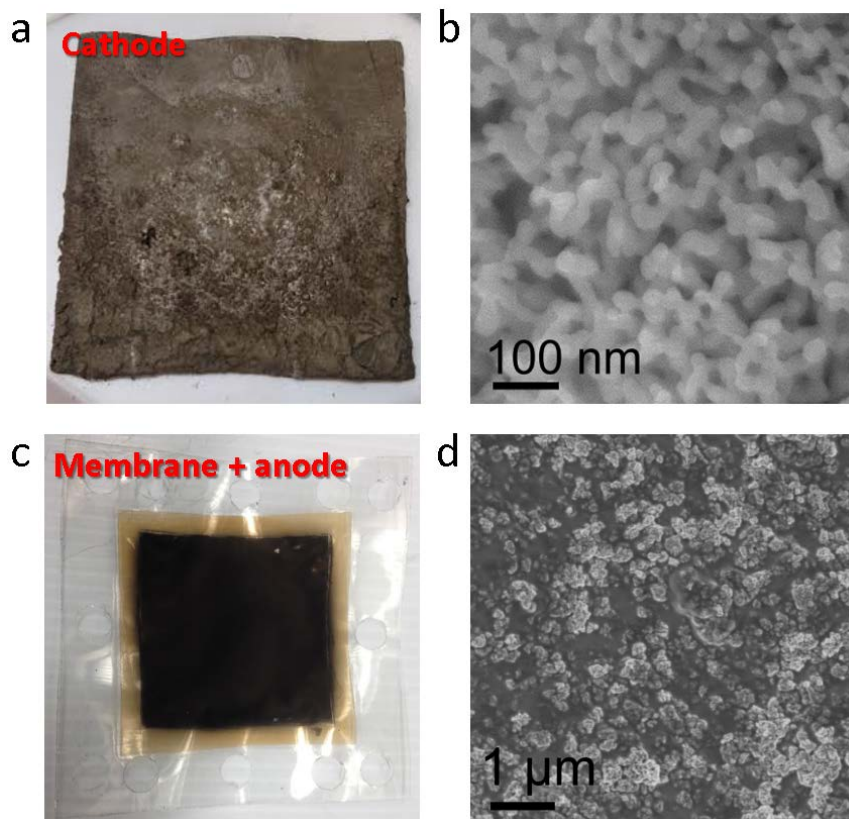
Figure 4.—CO$_2$ Electrolysis Cell Electrodes.
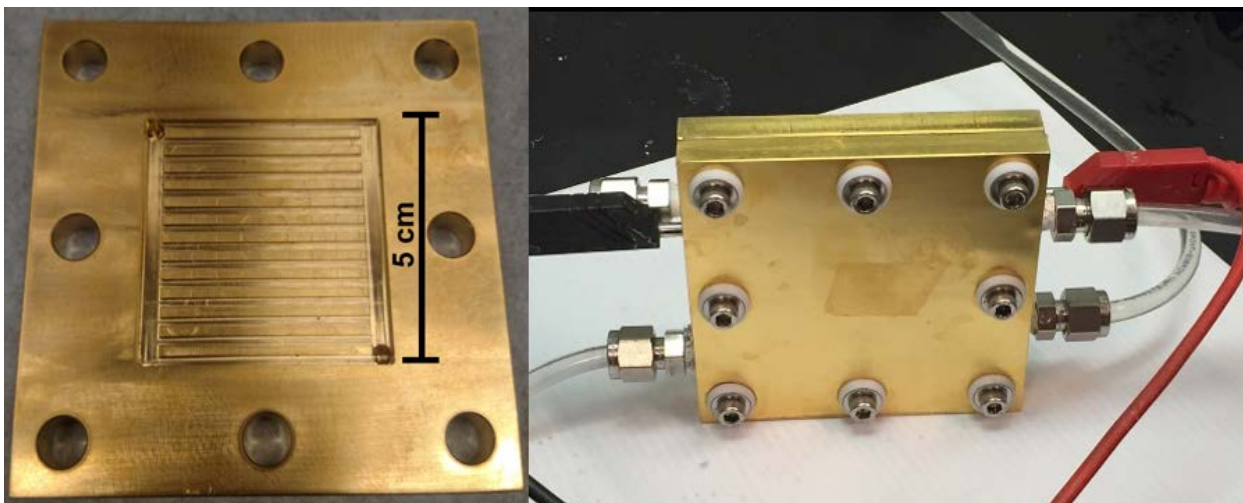
Figure 5.—CO₂ Electrolysis Flow Cell Gold Plated Stainless Steel Compartments.

2.1.2.3 Assembled 25 cm² Single CO₂ Electrolysis Flow Cell

Figure 5 show the assembled single 25 cm² CO₂ electrolysis flow cell. The end pieces were made of stainless steel, coated by a 2-µm layer of gold to prevent corrosion or other undesired reactions. Swagelok joints were used to connect catholyte and anolyte flows.

2.1.2.4 25 cm² Single CO₂ Electrolysis Flow Cell Testing Results

For the single flow cell experiments, the flow cell shown in Figure 5 was used. Nanoporous Ag was used as the cathode and Ir-coated Nafion membrane was used as the anode. An Autolab PGSTAT128N with 10A booster was used to control cell voltage. Constant potential electrolysis experiments were used to measure the current as a function of time. The catholyte flow rate was 150 mL min⁻¹. The CO₂ gas feeding rate (to the gas/liquid contactor) was set to 25 mL min⁻¹.

Figure 6 shows the performance of single CO₂ electrolysis flow cell. A CO Faradaic efficiency of ~80 percent was achieved at an applied potential of 2.2 to 3.0 V. The current increased as the applied voltage became higher. At 3.0 V, a total current of 1000 mA (40 mA/cm²) was achieved. This current density surpasses the key performance goal of 35 mA/cm². At 2.2 V, the cell current is nearly zero, so the cell voltage approximates the theoretical voltage of 1.34 V plus the sum of the cathode and anode overpotentials which would be 0.86 V. Based on this data, the cathode overpotential would be approximately half of the 0.86 V, or about 0.43 V which is below the key performance parameter goal of ≤0.6 V.

The single CO₂ electrolysis flow cell was also studied at prolonged test conditions. An applied voltage was set to 2.8 V. The catholyte flow rate was 150 mL min⁻¹ and the CO₂ gas feed rate was 25 mL min⁻¹. Figure 7 shows the current profile over the period of 120 hr of continuous operation. A decay of current was observed, while the CO Faradaic efficiency was relatively stable over the 120 hr. Following-up investigations suggest that the decrease of current is likely due to the cation exchange between Na⁺ in the catholyte and H⁺ in the Nafion membrane, which affected the proton conductivity across the membrane and thus led to a high internal resistance.
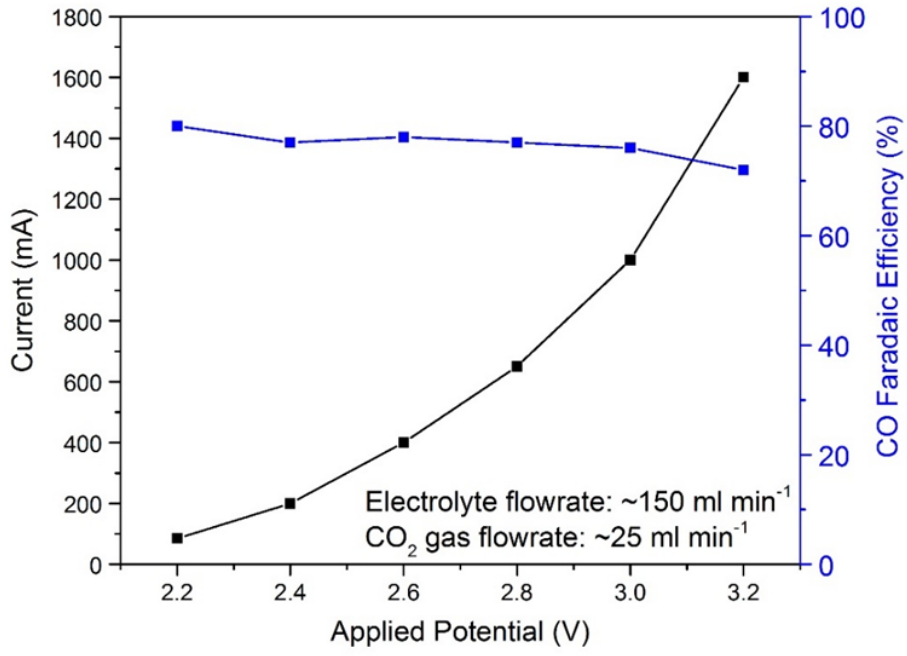
Figure 6.—Single 25 cm^2 CO$_2$ Electrolysis Flow Cell Electrochemical Performance.
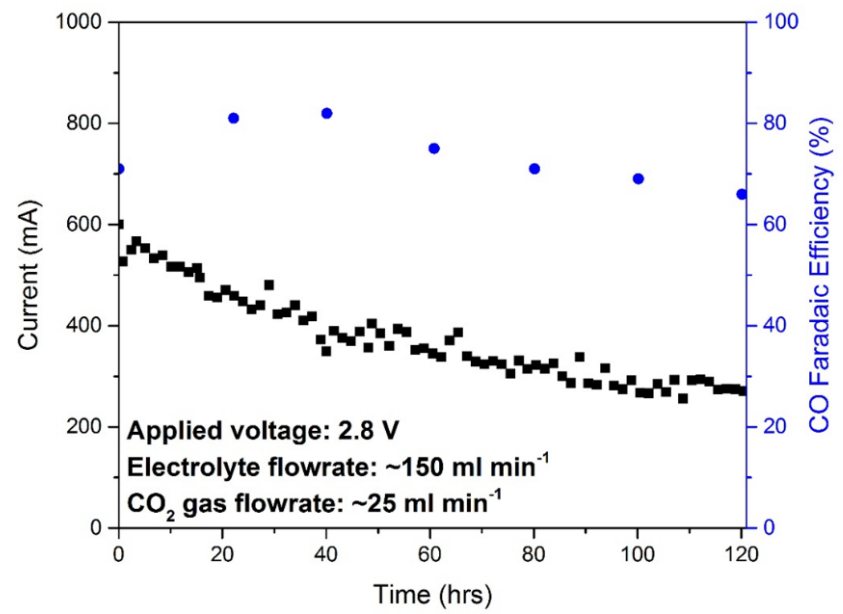
Figure 7.—Single 25 cm^2 CO$_2$ Electrolysis Flow Cell Long-Term Stability Test.

2.1.3   100 cm^2 Single CO$_2$ Electrolysis Flow Cell Development

The scale-up of the 25 cm^2 single CO$_2$ electrolysis cell to a 100 cm^2 single CO$_2$ electrolysis cell was investigated. The 100 cm^2 cell plate (Figure 8(a)) was designed and fabricated with similar materials as the 25 cm^2 cell plate. The 100 cm^2 nanoporous Ag electrode (Figure 8(b)) was also successfully fabricated using the same dealloying technique. In addition to the Ag electrode, a 100 cm^2 Ir-Coated Nafion as the oxygen evolution anode (Figure 8(c)) was also fabricated. The cell was assembled (Figure 9) and tested with a catholyte (0.5 M NaHCO$_3$) flow rate of 150 mL min^{-1} and CO$_2$ feed rate of 25 mL min^{-1}. The results are shown in Figure 10, which is similar to the performance of the 25 cm^2 cell studies. At an applied potential of 3 V, a total current of ~1900 mA with a CO Faradaic efficiency of 82 percent was achieved. Extrapolating the data to a current of zero, the cell voltage would be about 2.3 V which means the sum of the cathode and anode overpotentials would be 0.96 V. From this data, the cathode overpotential is approximately 0.48 V which meets the key performance parameter goal of ≤0.6 V.
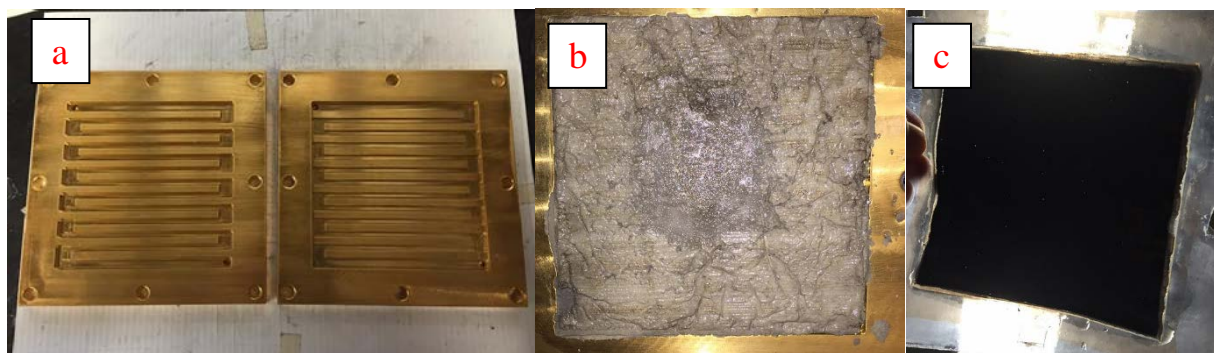
Figure 8.—100 cm^2 Single CO$_2$ Electrolysis Flow Cell Components. (a) 100 cm^2 Cell Plates (b) 100 cm^2 Cathode (c) 100 cm^2 Ir Coated Nafion Membrane.
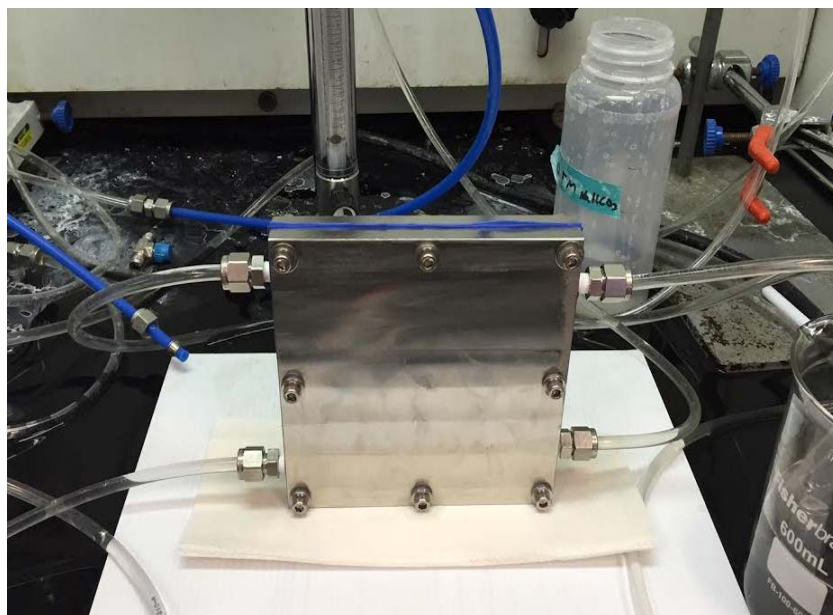
Figure 9.—Assembled 100 cm^2 Single CO$_2$ Electrolysis Flow Cell.
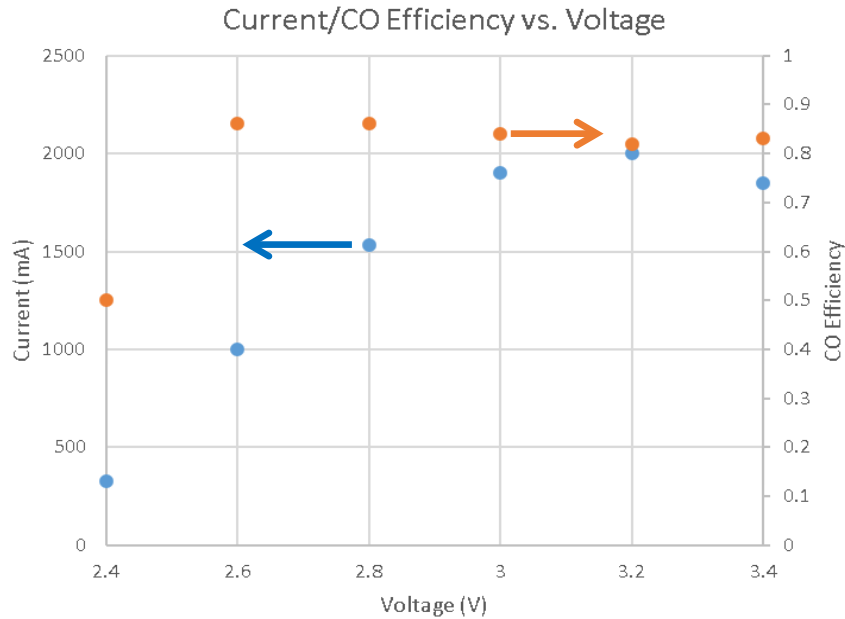
Figure 10.—The 100 cm² Single CO_2 Electrolysis Flow Cell Performance.
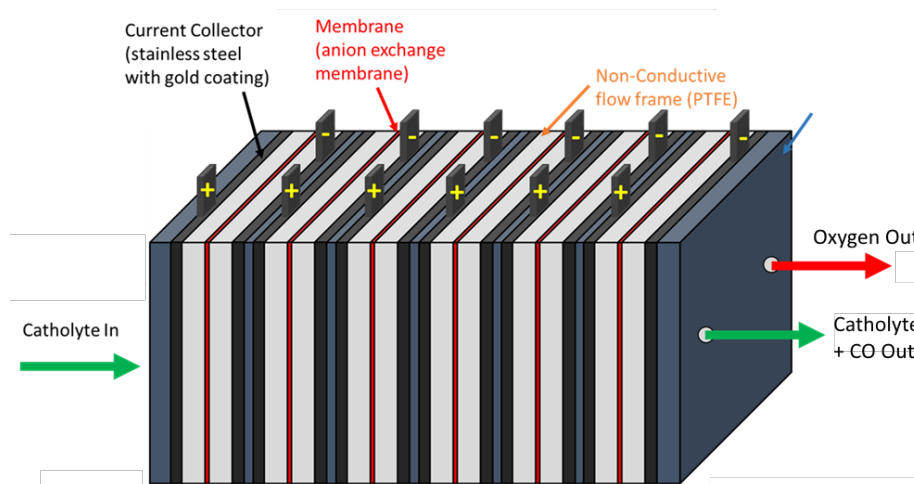
Figure 11.—Six Cell CO_2 Electrolysis Stack Design Illustration.

2.2   Six Cell Stack

2.2.1   Design

The overall design of the CO_2 electrolysis flow cell stack is shown in Figure 11. The six individual cells were connected electrically and fluidically in parallel and separated by a Teflon spacers. There was one port for catholyte to flow into the stack from one side of the stack and one exit port for the catholyte to flow out of the stack. On the anode side, there was no port for liquid flow in/out. The anode chambers were interconnected to an exit gas port for oxygen collection. The choices of electrode materials were the same as the single cell electrodes.

2.2.1.1 Electrode plate

Figure 12 is the engineering drawing of electrode plate design.

2.2.1.2 PTFE chamber

Figure 13 is the engineering drawing of PTFE chamber.
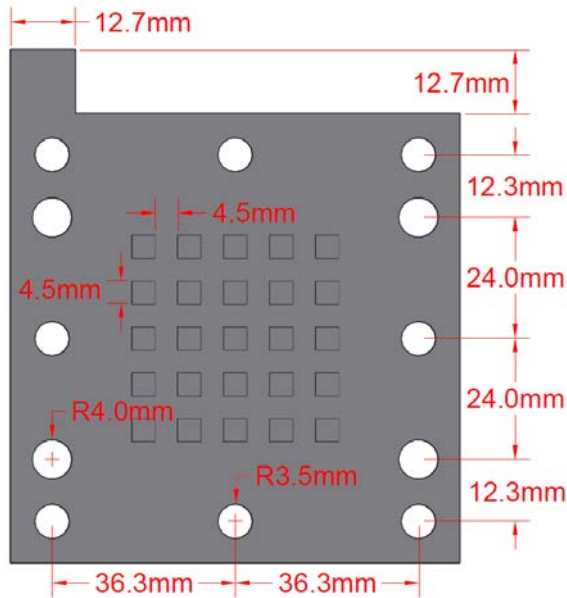
Figure 12.—Electrode Plate Design Engineering Drawing.
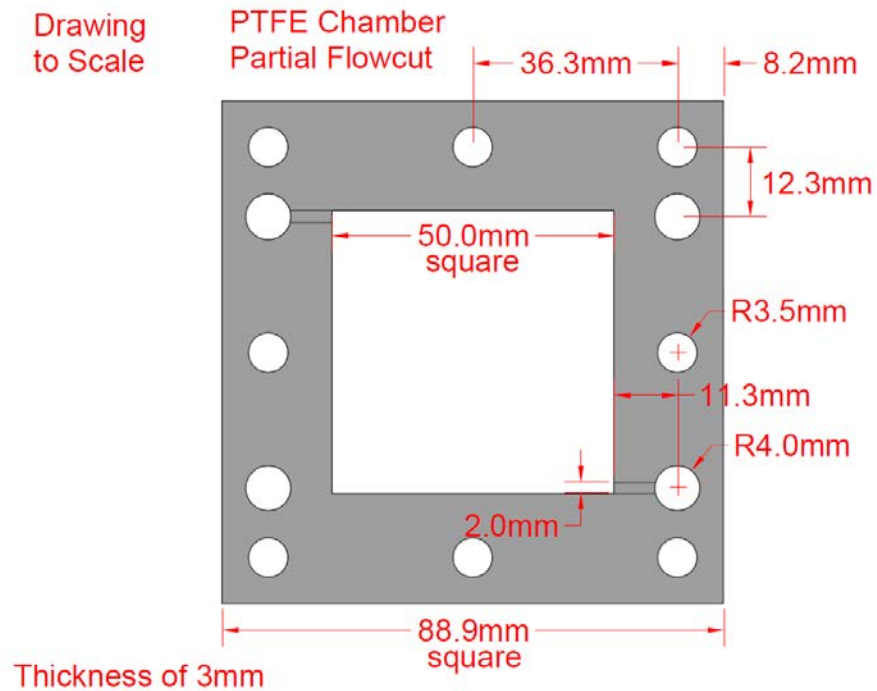
Figure 13.—PTFE Chamber Design Engineering Drawing.

2.2.1.3   PTFE Spacer

Figure 14 is the engineering drawing of PTFE spacer.
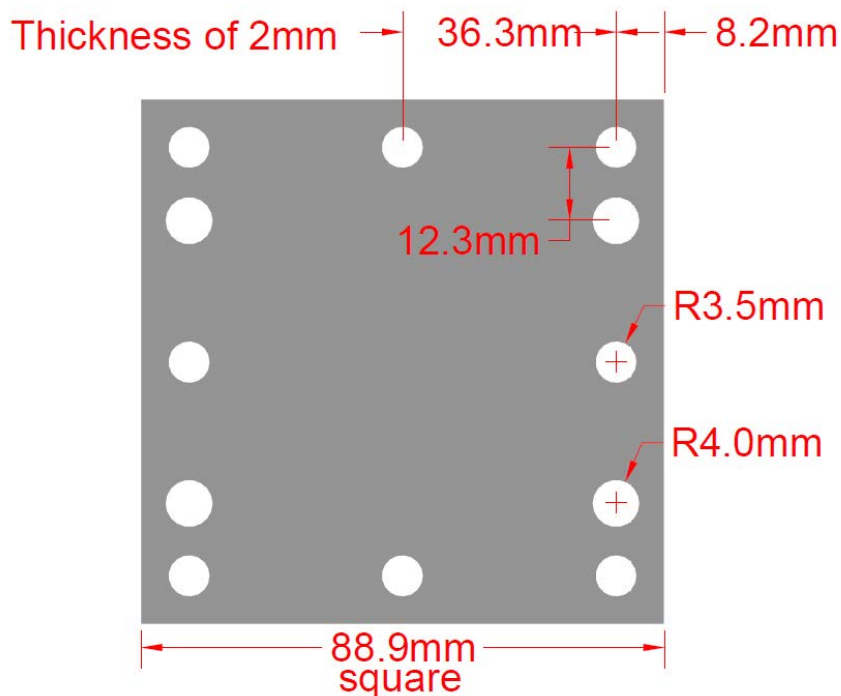
Figure 14.—PTFE Spacer Design Engineering Drawing.

2.2.2   Six Cell CO_2 Electrolysis Stack Fabrication

2.2.2.1   Nanoporous Ag Cathode

The fabrication of nanoporous Ag cathodes for the six cell stack was identical as the procedure for single cell.

2.2.2.2   Ir-Coated Nafion Membrane

The fabrication of Ir-coated Nafion membranes for the six cell stack was identical as the procedure for single cell.

2.2.2.3   Six Cell CO_2 Electrolysis Stack

The six cell electrolysis stack electrode plates with a pine-type flow pattern were made of stainless steel and coated with a layer of gold (2 μm thick). An as-fabricated electrode plate can be seen in Figure 15. A PTFE chamber part is shown in Figure 15(b).The fabrication of the PTFE Chamber parts and the PTFE Spacers was performed at Delaware Metal (Ref. 2).The silicon gaskets are shown in Figure 15(c) and (d). The holes in the gaskets were manually cut at University of Delaware. The quick joints shown in Figure 15(e) were purchased from Cole Parmer. The assembled six cell stack is shown in Figure 15(f).

2.2.3   Six cell CO_2 Electrolysis Stack Testing Results

The electrochemical performance of a six-cell CO_2 electrolysis stack is shown in Figure 16. The testing conditions were 150 mL min^{-1} of catholyte flow rate and the CO_2 gas feed rate of 20 mL min^{-1} at a pressure of 40 psi. The data was collected at 2.6, 2.8, and 3.0 V (applied voltage).
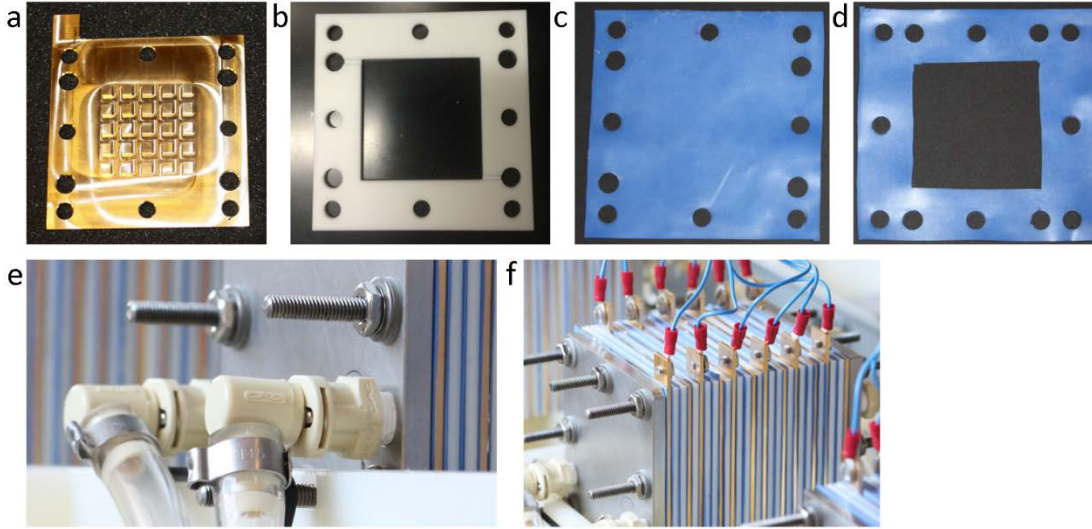
Figure 15.—Stack Cell Components: (a) Electrode Plate, (b) PTFE Chamber, (c) and (d) Silicon Gaskets, (e) Quick Joints for Electrolyte and Gas Ports, (f) Assembled Stack.

Cathode: np-Ag
Anode: Ir/Nafion XL, 1 mg cm^{-2}
Total Electrolyte Flowrate: 150 mL min^{-1}
CO_2 Gas Flowrate: 20 mL min^{-1} @ 40 psi

Single stack (6 cells)
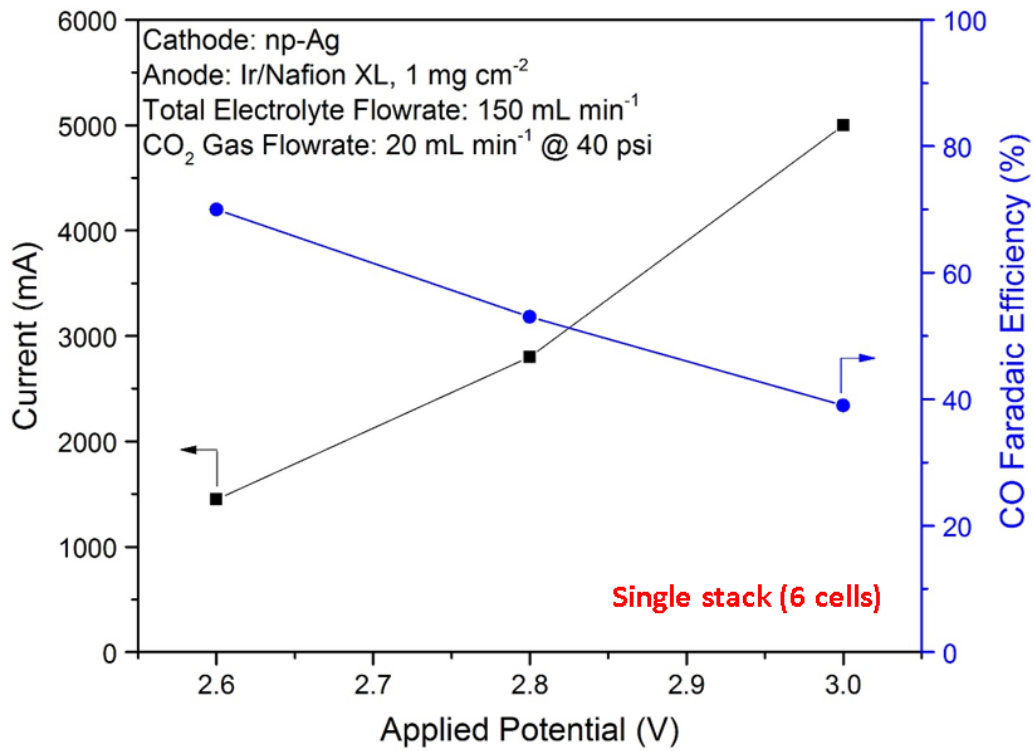
Figure 16.—Six Cell CO_2 Electrolyzer Stack Electrochemical Performance.
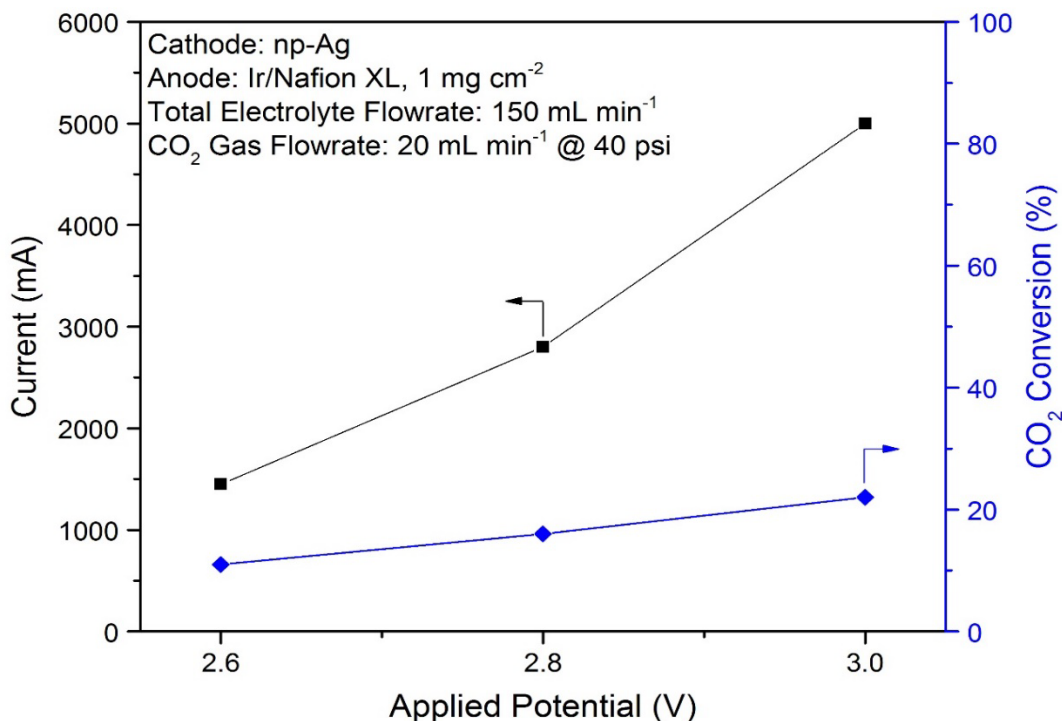
Figure 17.—Six Cell CO₂ Electrolyzer Stack Single Pass CO₂ Conversion.

Extrapolating the current to zero, the estimated stack voltage is 2.4 V. This means that the sum of the cathode and anode overpotentials was about 1.06 V. From this data, the cathode overpotential is approximately 0.53 V which is below the key performance parameter goal of $\leq 0.6$ V. A total current of 1.4 to 5.0 A (9.33 to 33.3 mA/cm²) was achieved which meets the threshold value for current density ≥ 25 mA/cm². The CO content of the exit gas was measured by a gas chromatograph, and compared to the theoretical maximum CO content that should exist if all of the stack current went to the production of CO. The ratio of the actual CO content of the exit gas to the theoretical maximum CO content is the CO Faradaic efficiency. The observed CO Faradaic efficiency for the six-cell test was around 40 to 70 percent. Extrapolating the data in Figure 16 to an applied potential of 2.5 V, the Faradaic efficiency exceeded the threshold goal of ≥ 80 percent. The difference between a 100 percent Faradaic efficiency and the observed efficiency is that percentage of the current that went to the production of hydrogen by water electrolysis.

The CO₂ conversion rate of the six-cell stack on a single pass was estimated by using the current and CO faradaic efficiency to calculate the total amount of CO reacted, which equals the amount of reacted CO₂. The amount of reacted CO₂ was divided by the CO₂ gas feed rate to get the single pass conversion rate. The results are shown in Figure 17. At the electrolyte flow rate of 150 mL min⁻¹ and CO₂ feed rate of 20 mL min⁻¹, the conversion was around 12 to 22 percent.

2.3 Carbon Dioxide Electrolyzer EDU

2.3.1 Design

The overall design of the CO₂ electrolyzer EDU is shown in Figure 18. The electrical portion of the design is shown in Figure 19. The six stacks were electrically and fluidically connected in parallel and connected to a gas/liquid contactor. The gas products are separated at a membrane based separator. The choices of electrode materials and stack components were the same as the single stack.

Figure 18 — P&ID CO₂ Electrolyzer (Sheet 1 of 9)

ITEM	QTY.	PART NO.	DESCRIPTION	ITEM	QTY.	PART NO.	DESCRIPTION
1	1		Catholyte Reservoir	6	2		Telltale Drain Vial
2	1		Gear Pump	7	6		Electrolyzer Stacks
3	1		CO2 Contactor	8	1		Gas Separator Stack
4	1		Flow Meter	9	1		Vent Valve
5	1		Catholyte Distribution Manifold	10			

P&ID
CO₂ Electrolyzer

SIZE Tab   WEC # 042816WEC   REV 0
SCALE NTS   SHEET 1 of 9
Approved:
Date Approved:

Figure 18.—CO₂ Electrolyzer EDU P&ID Schematic.

Figure 19 — Wiring Schematic

120 VAC
L1 (Black)

120 VAC
N (White)

Ground
G (Green) Connections Not Shown for Clarity

Emergency Stop — L1 — Eaton C25BNB230A — L2 — 2-Pole Contactor

T1   T2

Cole-Parmer 75211-10 — Catholyte Pump

Extra Pump Circuit

TDK-Lambda Z10-72-U — Stack DC Power Supply

+   -

CS1
CS2
CS3
CS4
CS5
CS6

CO2 Electrolyzer Stacks

Leviton Duplex GFI — Ground Fault Outlet

Leviton Duplex — Duplex Outlet

Wiring Schematic
CO₂ Electrolyzer

SIZE Tab   WEC # 042816WEC   REV 0
SCALE NTS   SHEET 1 of 9
Approved:
Date Approved:

Figure 19.—CO₂ Electrolyzer EDU P&ID Electrical Schematic.

A zero-gravity compatible gas/liquid separator was designed by the University of Delaware and NASA Glenn Research Center. Figure 20 is the engineering drawing of the gas/liquid separator. The separator is based on a porous hydrophobic PTFE membrane.

2.3.2 CO₂ Electrolyzer EDU Fabrication

The as-fabricated CO_2 Electrolyzer EDU is shown in Figure 21. The EDU has three stages, the electronic stage, the electrolyzer stage, and the plumbing stage.
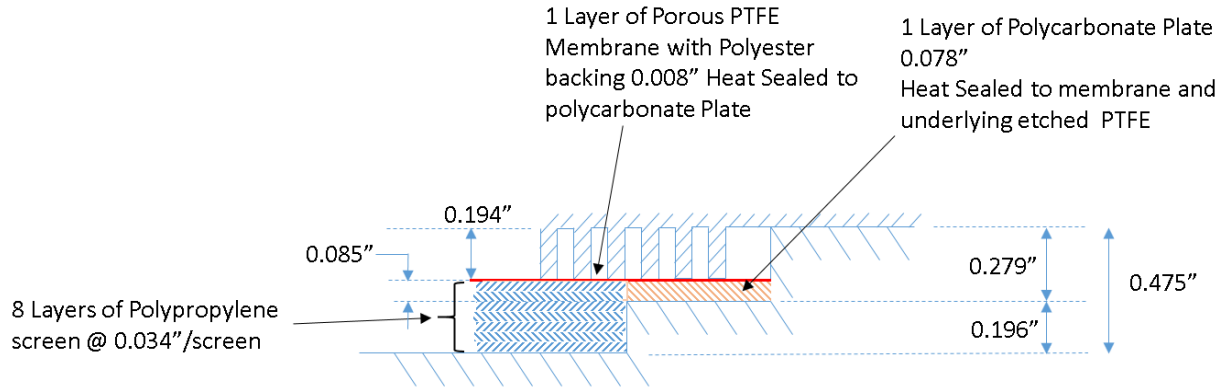
Figure 20.—Gas/liquid Separator Engineering Drawing.
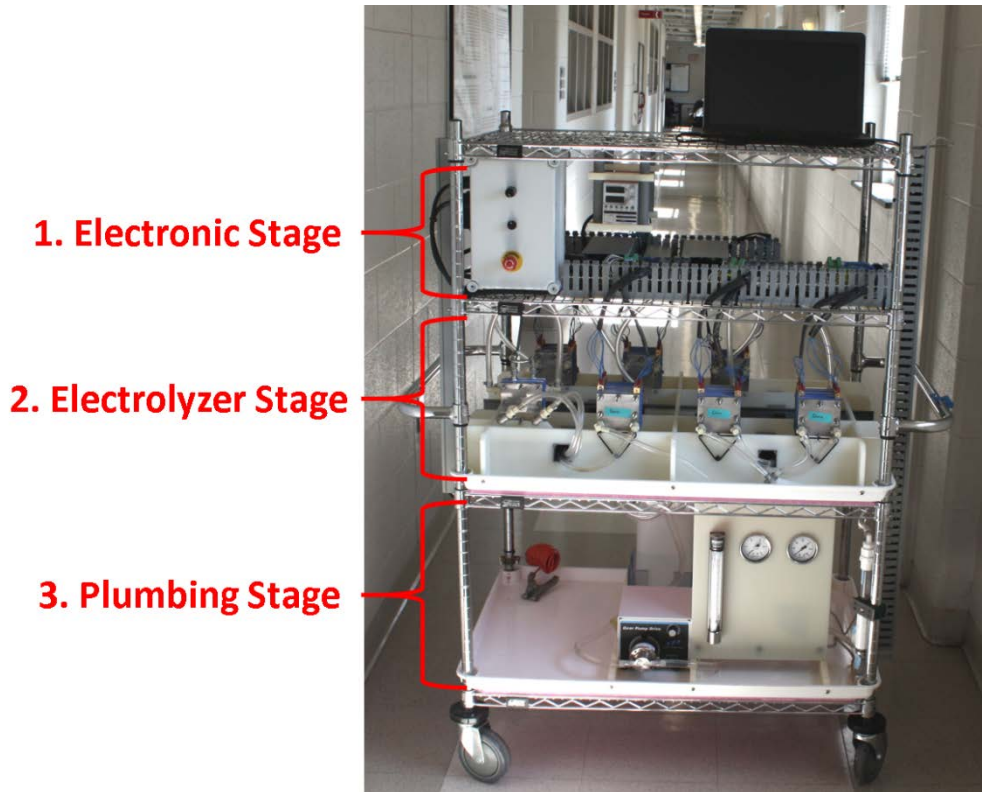
Figure 21.—CO₂ Electrolyzer EDU.

2.3.2.1 Electronic Stage

A front view of the electronic stage of the EDU is shown in Figure 22. A laptop was used for data collection and electrochemical performance monitoring. The power box contained power outlets and an emergency stop switch as a safety feature. The power supply was used to set the applied voltage to the EDU. A digital displayer for the total current was also on the front panel of the power supply. Six chip boards together with a unit from National Instrument were placed in the electronic stage to collect the current readings from the stacks in the electrolyzer stage. A side view of the electronic stage of the EDU is shown in Figure 23. In the side view, a flammable gas alarm can be seen. This was a safety feature to detect any flammable gas leakage because CO and H_2 are produced in the EDU. A LabVIEW (National Instruments) software was built for the EDU data acquisition, collection, and storage. Figure 24 is a screen shot of the software user interface. The software can display six stacks in one window and within each stack, the software can display each individual cell performance. The current data was saved to the laptop every 10 sec.
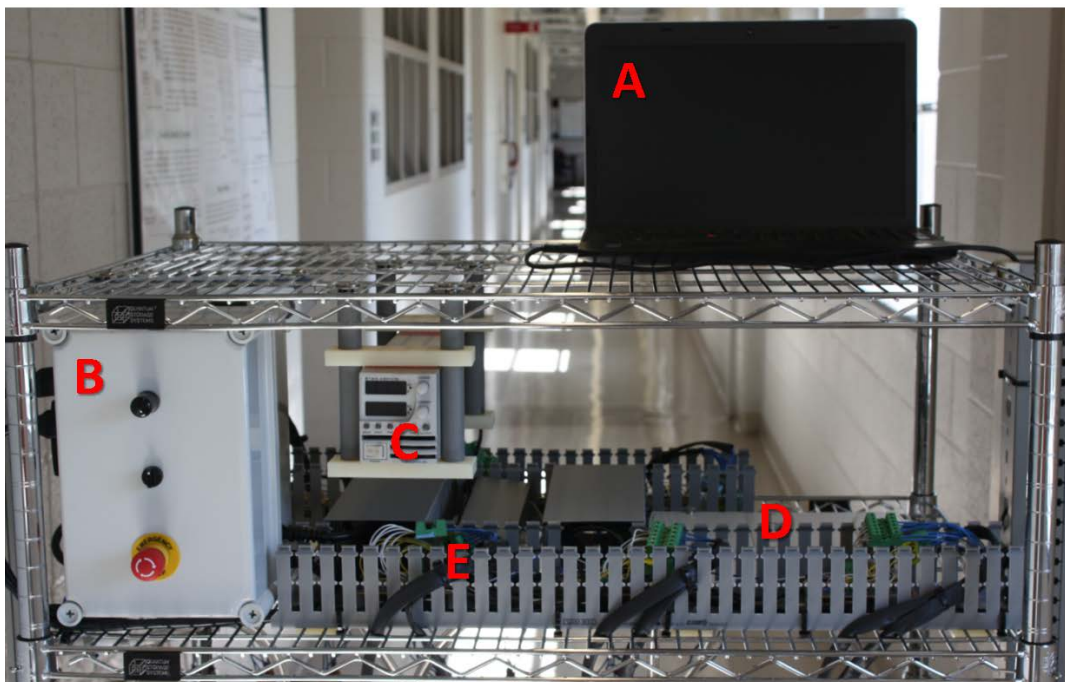
A: Laptop (data collection and monitoring); B: Power box (power outlets, emergency stop);
C: Power supply; D: National instrument unit; E: Chips for current measurement

Figure 22.—CO$_2$ Electrolyzer EDU Electronic Stage Front View.
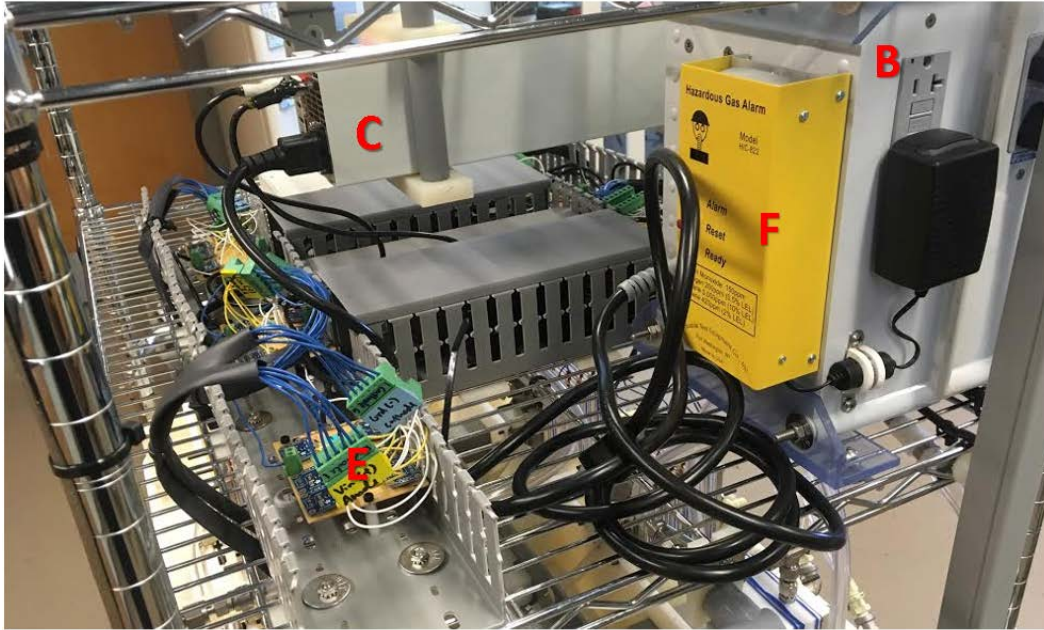
B: Power box (power outlets, emergency stop); C: Power supply; E: Chips for current measurement; F: Flammable gas alarm (CO and H_2 sensors)

Figure 23.—CO_2 Electrolyzer EDU Electronic Stage Side View.
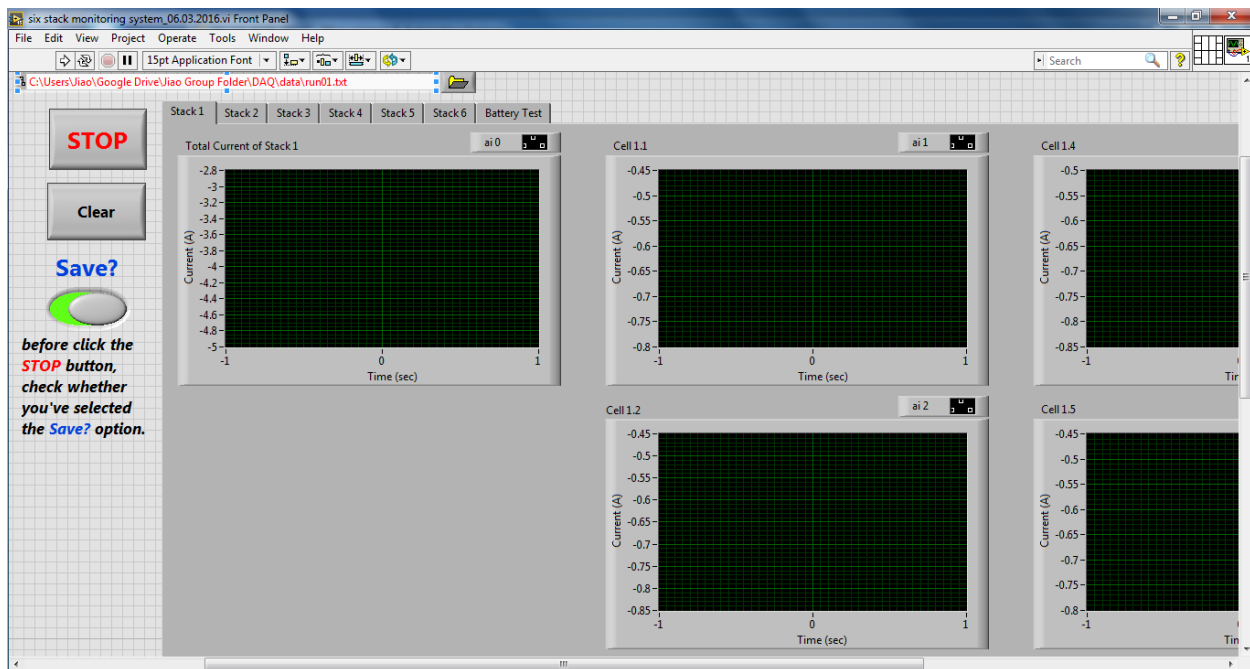
Figure 24.—Customized LabVIEW Software for EDU Data Acquisition.

2.3.2.2   Electrolyzer Stage

The front view of the EDU electrolyzer stage is shown in Figure 25. Six six-cell stacks were electrically and fluidically connected in parallel. One membrane based gas/liquid separator was connected to the catholyte stream. Quick joints were used for easy disassembly/re-assembly.

The as-fabricated gas/liquid separator is shown in Figure 26. The as-assembled separator was tested for gas and liquid leakage before connecting to the whole EDU.
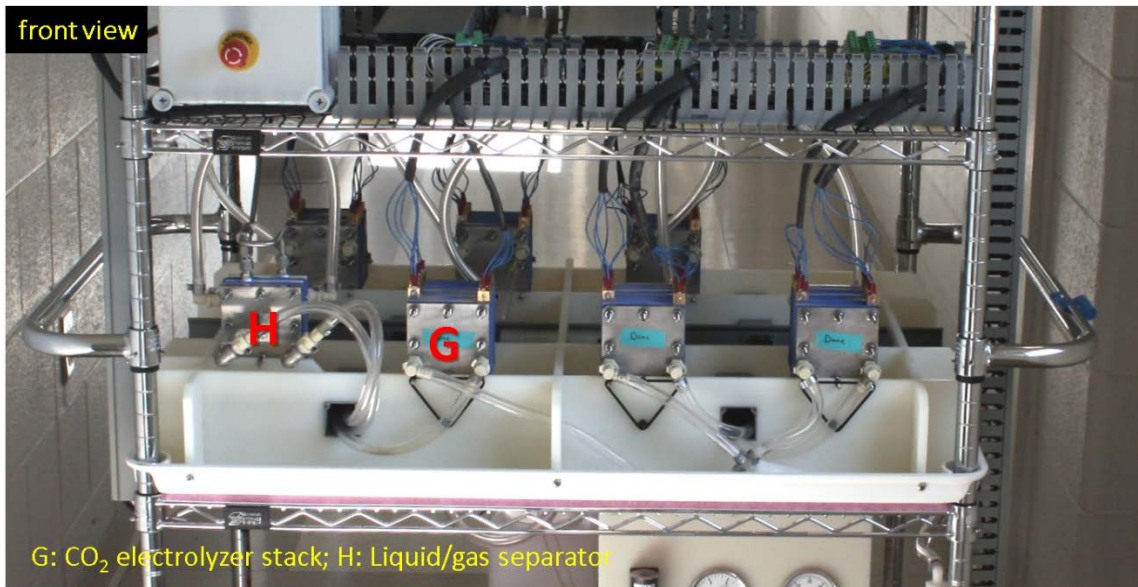
Figure 25.—CO$_2$ Electrolyzer EDU Electrolyzer Stage Front View.
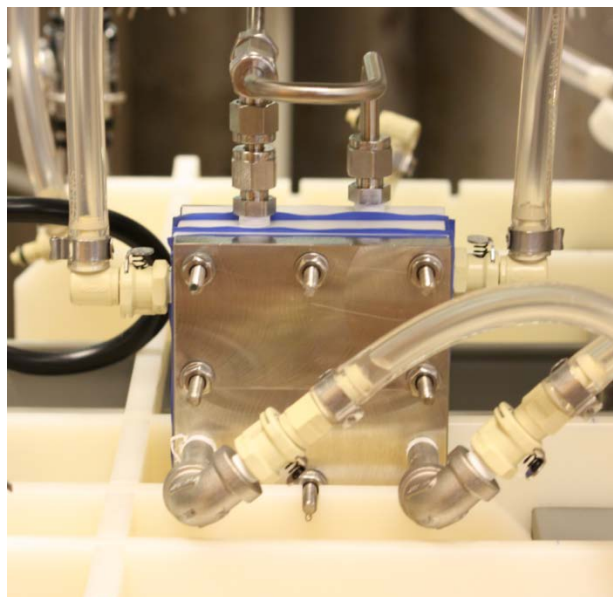
Figure 26.—CO$_2$ Electrolyzer EDU Gas/Liquid Separator.
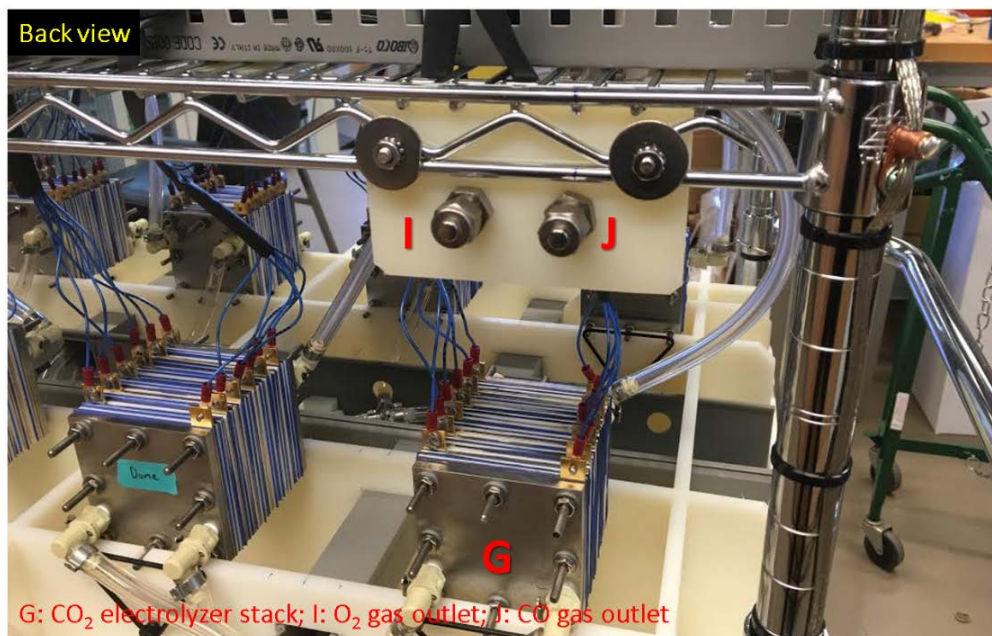
Figure 27.—CO₂ Electrolyzer EDU Electrolyzer Stage Back View.

The back view of the EDU electrolyzer stage is shown in Figure 27. Two gas outlets were provided, one for CO and the other for O_2.

2.3.2.3   Plumbing Stage

The front view of the EDU plumbing stage is shown in Figure 28. Several key components for electrolyte circulation, gas/liquid mixing and pressure monitoring were placed on the plumbing stage.

The back view of the EDU plumbing stage is shown in Figure 29. A Swagelok connection was provided for CO_2 gas supply. A tray is in place to prevent potential chemical spills. The electrolyte tank has a pressure release valve on the top.

2.3.3   CO₂ Electrolyzer EDU Testing Results

The assembled EDU was tested under various applied potentials from 2.7 to 3.0 V. The total catholyte flow rate was set to 1800 mL min^{-1} and the CO_2 gas feed rate was 150 mL min^{-1} at a delivery pressure of 40 psi. The results are shown in Figure 30. At an applied voltage of 3.0 V, a total current of 20 A was achieved. Extrapolating the data in Figure 30 to an actual applied voltage of 3.1 V the current is 22.5 A which is the threshold value of ≥ 25 mA.cm^2. Likewise extrapolating data in Figure 30 to an applied voltage of 2.6 V, the EDU meets the threshold level for Faradaic efficiency of ≥ 80 percent. Lastly, if the data in Figure 30 is extrapolated to zero current, the applied voltage would be near 2.3 V, which, after subtracting the theoretical voltage of 1.34 V, leaves 0.96 V for the sum of the overpotentials at the cathode and anode. The cathode overpotential is estimated to be approximately 0.48 V, which meets the goal value of ≤ 0.6 V. The potentials in red are the actual applied voltage, while the numbers in black are the readings from the power supply.

The customized LabVIEW software also recorded the performance of each individual six-cell stack. The voltage for each of the six-cell stacks was set to 2.7, 2.8, 2.9, and 3.0 V for each step. As the voltage was increased stepwise, the current observed from each of the stacks increased also in a stepwise fashion. The current at 2.7 V was the lowest while the current at 3.0 V was the highest. The results can be seen in Figure 31. Stack 5 showed the highest currents, which made it the best performing stack, while Stack 3 showed the lowest currents. The variation in performance is likely due to the cell component quality.
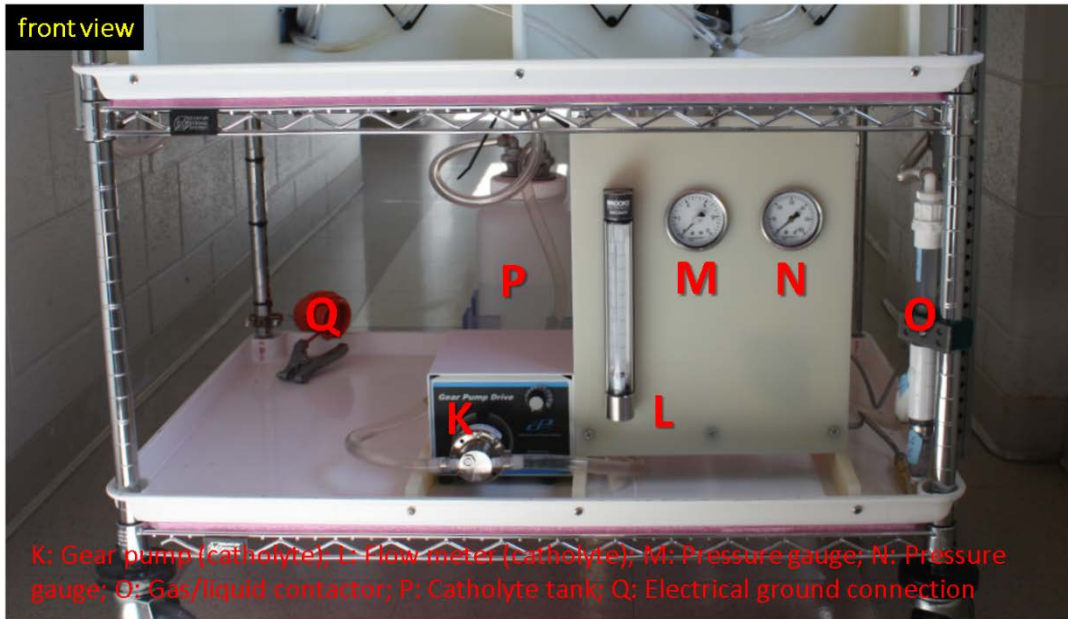
Figure 28.—CO₂ Electrolyzer EDU Plumbing Stage Front View.
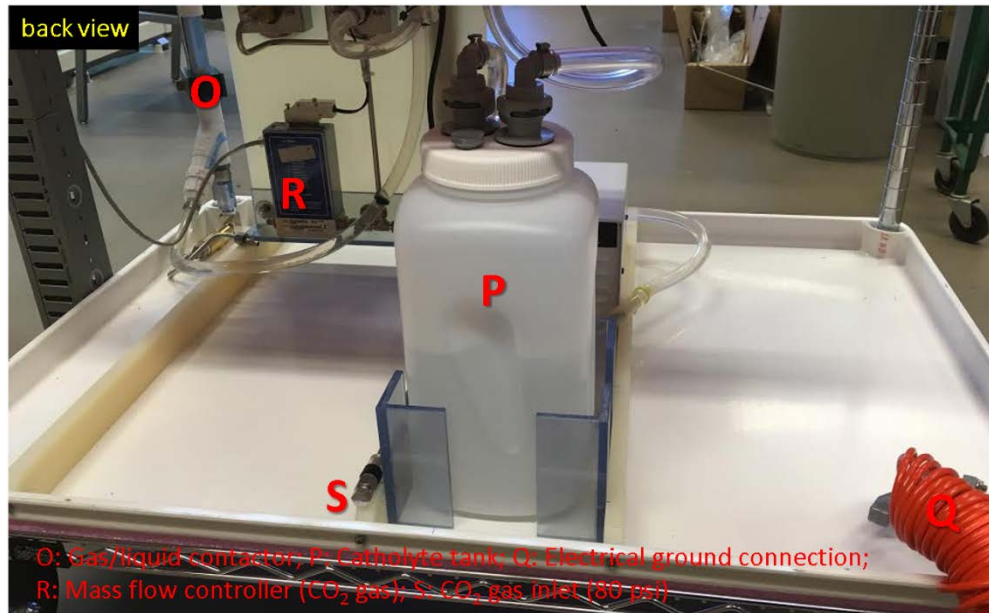
Figure 29.—CO₂ Electrolyzer EDU Plumbing Stage Back View.
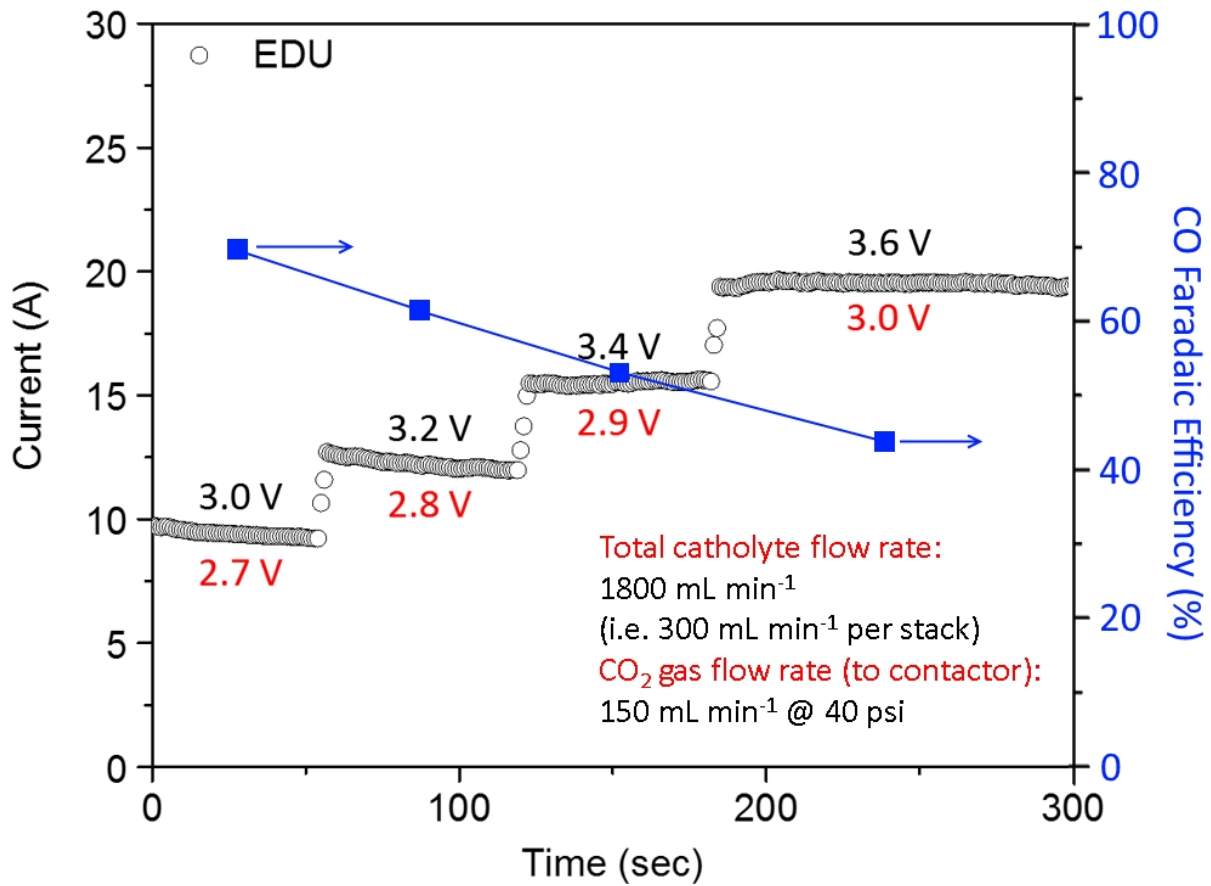
Figure 30.—CO_2 Electrolyzer EDU Electrochemical Performance.
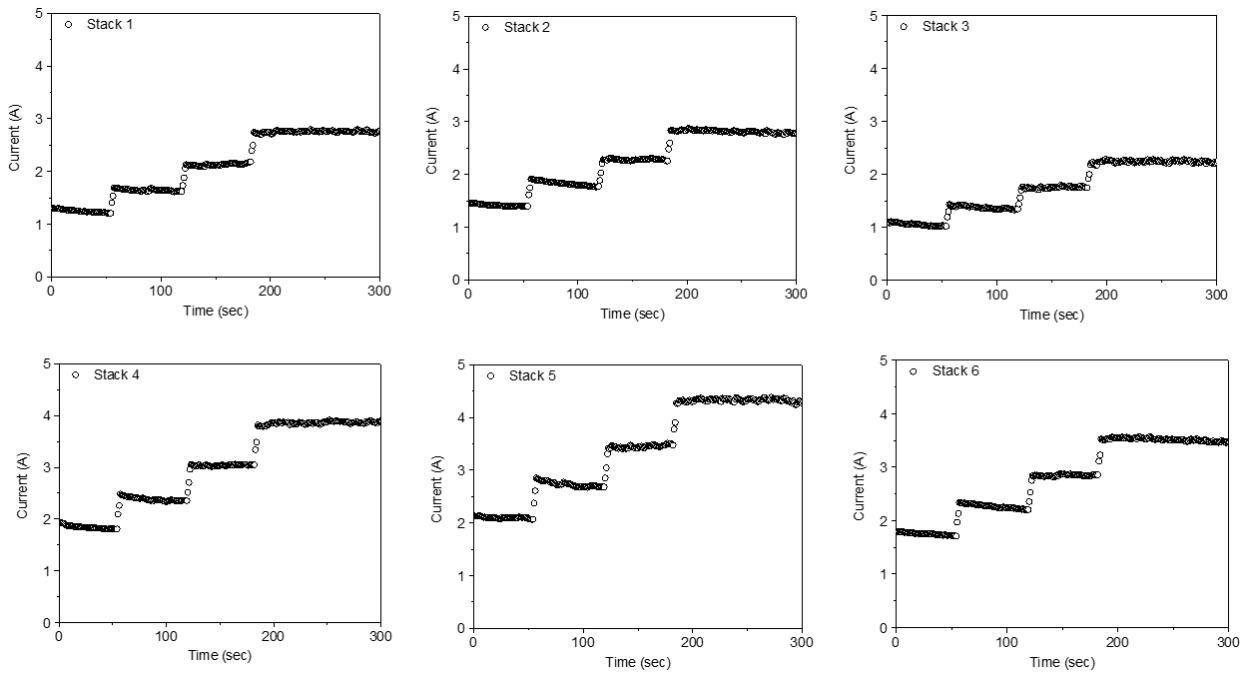
Figure 31.—CO_2 Electrolyzer EDU Electrochemical Performance of Six Cell Stacks.

3.0   Carbon Monoxide Catalytic Conversion

For near complete recovery of oxygen from carbon dioxide the carbon monoxide from the carbon dioxide electrolysis process needs to be coupled with a process that removes carbon from the system, giving the overall reaction:

$$CO_{2(g)} \rightarrow C_{(s)} + O_{2(g)}$$
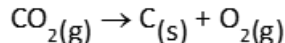
Carbon monoxide can either molecularly adsorb or dissociate on a catalytic surface depending on the chemistry, temperature and pressure. Under specific process conditions, dissociation leads to deposition according to the Boudouard reaction:

$$2CO\,(g) \rightarrow C(s) + CO2(g) \quad \Delta H^\circ rxn = -172\ kJ/mole$$
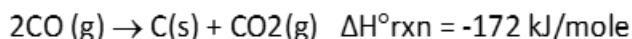
where surface carbon is in the form of a carbide species, as amorphous carbon, graphite or carbon nanofibers (Ref. 3). One key advantage of the Boudouard reaction is that its equilibrium favors carbon deposition at temperatures lower than the Bosch (650 °C) or lower than Solid Oxide CO_2 electrolysis (850 °C) reactions that could be used in the reclamation of oxygen from CO_2. The CO_2 can then be recycled back into the electrolysis process for further oxygen recovery. The objective of this portion of the work was to develop a reactor that removes carbon from the system by catalytic disproportionation of carbon monoxide (Boudouard reaction) and safely retain the carbon inside the reactor prior to its safe removal from the reactor.

3.1   Carbon Monoxide Catalyst

Metals such as iron, nickel, cobalt and ruthenium adsorb carbon monoxide on their surfaces. Of these metals, iron is the least expensive on Earth and is a common component of asteroid, lunar, and Martian regolith, so could provide a mission based resource. Among metal carbonyls, carbon forms the strongest bond with iron. Iron has a particularly strong affinity for carbon monoxide and has a strong activity for the Boudouard reaction (Refs. 4 to 6). This work concentrated on iron-based materials as the catalytic surface for carbon disproportionation.

3.1.1   Non-Steel Wool Catalyst Screening

Initial efforts to catalyze the Boudouard reaction were focused on the use of iron and iron oxide pellets. Pure powders were pressed in a Carver Press at 5000 psi to form substantial disks that could be run in the test furnace. Powders of 40 mesh iron (Fisher I-57) and 5 micron iron (III) oxide (Cerac I-1077) were used in this process. Some of these disks were sintered to 1100 °C. All samples were stored at 110 °C to keep them dry to avoid ambient surface oxidation through interaction with humidity. All samples were heated in the growth furnace to growth temperature under inert gas to remove binders and lubricant. These samples were then used to explore the growth parameters from 400 to 500 °C and with carbon monoxide or carbon monoxide with 5 percent hydrogen. Visual observation results ranged from bluish discoloration to small amounts of black mottling. These samples were examined with a Scanning Electron Microscope (SEM) and with Energy Dispersive X-ray Spectroscopy (EDS) to look for the form and placement of any carbon on the samples. This did confirm carbon deposition. However, the amount was never significant. Figure 32 shows SEM images of growth on an iron pellet. The growth occurred at 400 °C in CO for 5 hr. EDS mapping showed the existence of surface carbon on the pellet, though the amount of growth on the sample was minimal.
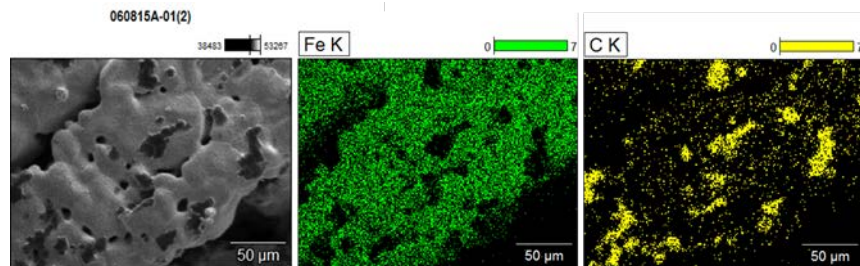
Figure 32.—SEM and EDS Images of Non-Steel Wool Catalysts.

TABLE 1.—STEEL WOOL CATALYST TESTING RESULTS

Sample	7-20-15A	7-31-15A	8-4-15A	8-6-15A	8-25-15A	8-28-15A	9-16-15A	9-22-15A	9-29-15A	10-6-15A	10-8-15A	10-27-15A 600C
CO flow (sccm)	475	475	475	475	475	475	47.5	47.5	145.5	145.5	291	291
Duration (min)	120	120	407	120	420	120	130	67	450	420	720	120
Volume flowed (cc)	57000	57000	193325	57000	199500	57000	6175	3183	65475	61110	209520	34920
Moles flowed (mol)	2.544	2.544	8.627	2.544	8.902	2.544	0.276	0.142	2.922	2.727	9.350	1.558
Mass gaseous C (g)	30.551	30.551	103.619	30.551	106.929	30.551	3.310	1.706	35.094	32.754	112.300	18.717
Catalyst mass (g)	1.304	0.680	2.468	1.433	0.380	1.578	1.0774	0.5397	1.1286	1.0954	1.034	1.0978
Est. Catalyst Bulk Volume, (cc) (2)	28.25	14.73	53.45	31.02	8.24	34.16	23.33	11.69	24.44	23.72	22.39	23.77
Est. Catalyst Dense Volume, (cc) (1)	0.17	0.09	0.31	0.18	0.05	0.20	0.14	0.07	0.14	0.14	0.13	0.14
Out mass (g)	5.88	5.20	20.93	5.12	10.79	7.01	1.76	0.70	6.06	12.47	21.52	2.61
C growth mass (g)	4.58	4.52	18.46	3.69	10.41	5.43	0.6867	0.16	4.93	11.37	20.48	1.51
Carbon/Catalyst g/g	3.51	6.64	7.48	2.58	27.37	3.44	0.64	0.29	4.37	10.38	19.81	1.38
Est Carbon Growth Volume, (cc) (3)	2.29	2.26	9.23	1.84	5.21	2.71	0.34	0.08	2.46	5.69	10.24	0.76
Combined Volume of Steel + Carbon, (cc)	2.45	2.35	9.55	2.03	5.25	2.92	0.48	0.15	2.61	5.83	10.37	0.90
Est Combine Catalyst + Carbon Porosity, %	91.31	84.08	82.14	93.47	36.23	91.47	97.94	98.74	89.33	75.44	53.68	96.23
Est Rate of Carbon Deposition, g C/g cat/hr	1.75	3.32	1.10	1.29	3.91	1.72	0.29	0.26	0.58	1.48	1.65	0.69

(1) Based on Steel Density of 7.87 gram/cc
(2) Based on Bulk Steel Wool Density of 0.046 g/cc
(3) Based on Amorphous Carbon Density of 2.0 g/cc

3.1.2   Steel Wool Catalyst Screening

Previous work by others (Refs. 7 to 9) for the development of Bosch carbon formation reactors had used steel wool as the catalyst material. Tests for this project were run in a laboratory tubular furnace with steel wool. These tests were run to evaluate the effectiveness of the steel wool catalyst relative to the other tested catalysts as well as to evaluate the effects of temperature, time, and catalyst sample size. The initial tests with steel wool showed substantial superiority of performance compared to the other catalysts tested. All subsequent catalyst testing was done with steel wool as the catalytic material. Table 1 summarizes the results of that testing.
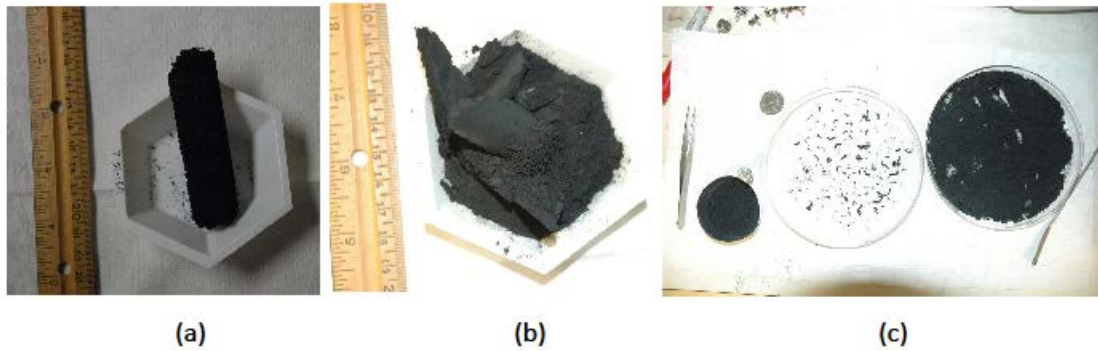
Figure 33.—Carbonized Steel Wool Catalyst Samples.

The samples shown in Figure 33(a), (b), and (c) are from the tests 7-20-15A, 8-04-15A, 8-25-15A, respectively described in Table 1.

The Key Performance Parameters (KPP) that were identified in the Phase I proposal are compared to the results of each steel wool sample tested in Table 2. In general the threshold levels for all the KPPs related to the carbon monoxide catalysts were met, and many of the samples met the goal levels for both carbon deposition rate and the carbon deposition per gram of catalyst. Because of the success of the steel wool to meet the project's goals, no further testing of alternate catalysts was performed during Phase I.

TABLE 2.—STEEL WOOL CATALYST PERFORMANCE COMPARISON WITH KPP'S

Key Performance Parameter	7-20-15A	7-31-15A	8-4-15A	8-6-15A	8-25-15A	8-28-15A	9-16-15A	9-22-15A	9-29-15A	10-6-15A	10-8-15A	10-27-15A 600C
Carbon Deposition Rate												
Threshold ≥ 0.2 gCarbon/gCatalyst/hr	Met	Met	Met	Met	Met	Met	Met	Met	Met	Met	Met	Met
Goal ≥ 0.4 gCarbon/gCatalyst/hr	Met	Met	Met	Met	Met	Met	Not Met	Not Met	Met	Met	Met	Met
Carbon Deposition												
Threshold ≥ 2.0 gCarbon/gCatalyst	Met	Met	Met	Met	Met	Met	Not Met	Not Met	Met	Met	Met	Not Met
Goal ≥ 4.0 gCarbon/gCatalyst	Not Met	Met	Met	Not Met	Met	Not Met	Not Met	Not Met	Met	Met	Met	Not Met
Operating Temperature												
Threshold ≤ 600°C	Met	Met	Met	Met	Met	Met	Met	Met	Met	Met	Met	Met
Goal ≤ 350°C	Not Met	Not Met	Not Met	Not Met	Not Met	Not Met	Not Met	Not Met	Not Met	Not Met	Not Met	Not Met

3.2   Carbon Monoxide Catalytic Conversion EDU

The Carbon Monoxide Catalytic Conversion (CMCC) EDU was the culmination of the carbon formation reactor work in Phase I. This EDU incorporated the knowledge gained from the catalyst screening tests as well as information obtained from the review of prior work done by others (Refs. 7 to 9) who were developing technology for a Bosch reactor for carbon dioxide reduction for aerospace applications.

The design of the Bosch reactors produced by others generally shared the following characteristics:

- Spent catalyst and the carbon deposited on the catalyst were removed by cooling the reactor to allow for partial reactor disassembly to gain access to the accumulated carbon,
- Upon reactor disassembly, the carbon, typically in a "catalyst cartridge" was removed, and the reactor was reloaded with another cartridge, then reassembled
- Upon reassembly, the reactor was re-heated and normal operations were resumed.
- No work was done to address the post unloading containment of the expelled carbon-laden catalyst.

These Bosch reactors had several disadvantages that this project wanted to address and, if possible, overcome. These disadvantages were:

- Cooling and reheating of the reactor in order to perform routine cartridge change-outs because this requires a dual reactor which adds both extra mass and volume.
- The cooling/re-heating puts an extra burden on the spacecraft cooling and power systems.
- The cooling/re-heating is time consuming. Hours are needed for just the cooling and re-heating.
- The cooling/re-heating is generally hard on material longevity.
- The manual disassembly/re-assembly process did not lend itself to automation, was prone to leakage introduction, and produced a significant risk that containment of the fine particulate carbon could be lost, exposing both crew and equipment to contamination.

The design of the EDU built incorporated several feature that overcome that above disadvantages. These design features are:

- The routine catalyst change-out did not require the reactor to be cooled/re-heated. The reactor stayed at its nominal operating temperature during these operations.
- The time needed for loading and unloading of catalyst/carbon from the reactor is only a few minutes for each operation, so downtime is minimal.
- Only minor disassembly is needed to position a fresh catalyst sample in the servicer section of the reactor assembly or remove spent catalyst material. This minimizes operator exposure to carbon particle release.
- The unloaded catalyst/carbon material was contained in a sealed receiver chamber that prevented the release of fine carbon particles. This containment allows for either a long term storage strategy or catalyst re-use strategy to be developed and implemented in the future.
- Much of the loading and unloading operation can be automated.

The operation of the EDU was primarily manual. This was intentional so that project resources were not spent in troubleshooting automation/software. A purge box surrounded the EDU. The purge box was purged with ventilation air at a rate that "turned over" the air inside the purge box three times per minute. This prevented any gas leakage from the reactor to escape into the laboratory or to accumulate to unsafe levels. The purge box consisted of an aluminum cage that was covered with clear polycarbonate panels. The polycarbonate panels on the "front" of the EDU were hinged to allow the panels to be opened when necessary during the operation of the EDU. Figure 34 and Figure 35 show the EDU from the front and rear respectively. A close up view of the Reactor Assembly inlet gas side and the Reactor Assembly outlet gas side are shown in Figure 36 and Figure 37, respectively. The P&ID and Electrical Schematic for the CMCC EDU are in Appendix A.—CMCC EDU P&ID and Electrical Schematics.
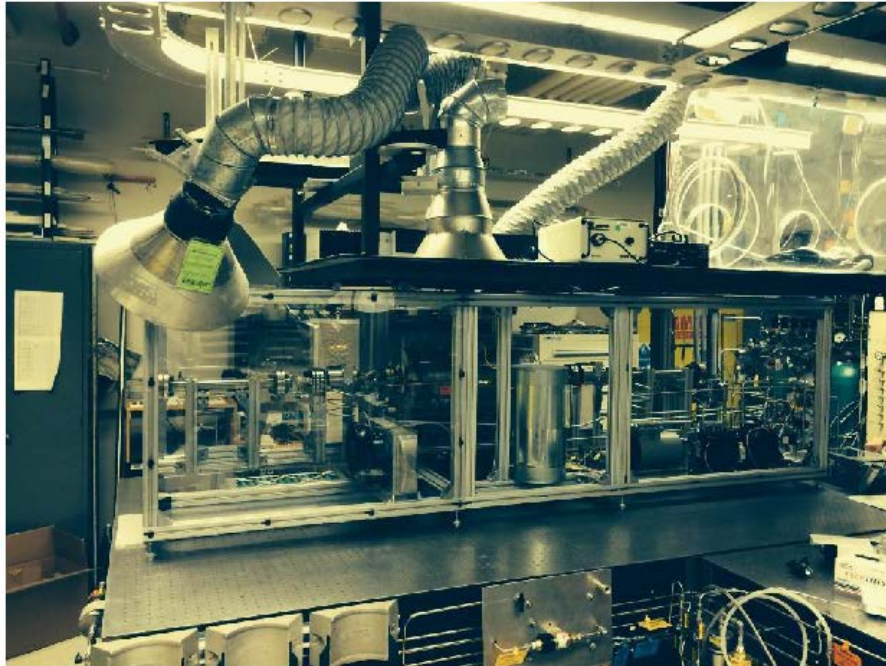
Figure 34.—CMCC EDU Rear View.
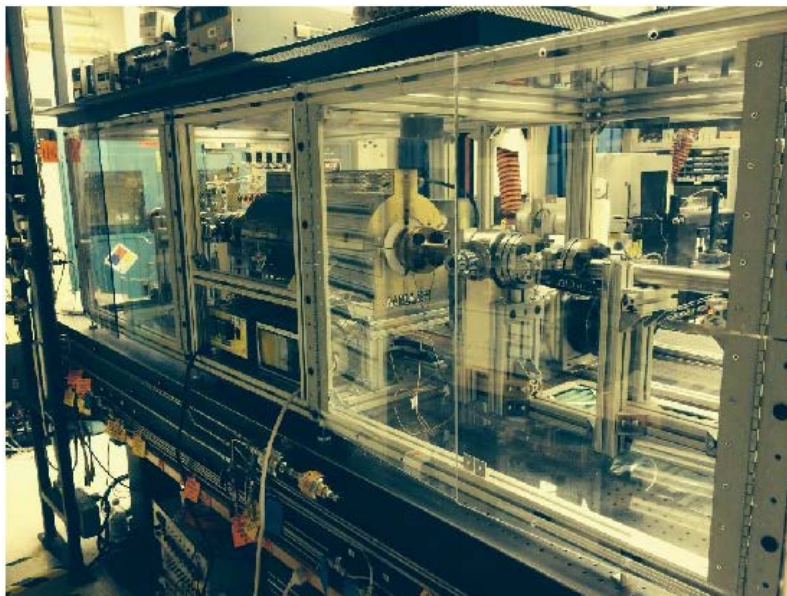
Figure 35.—CMCC EDU Front View.

Figure 36.—CMCC EDU Reactor Assembly Inlet Gas Side.
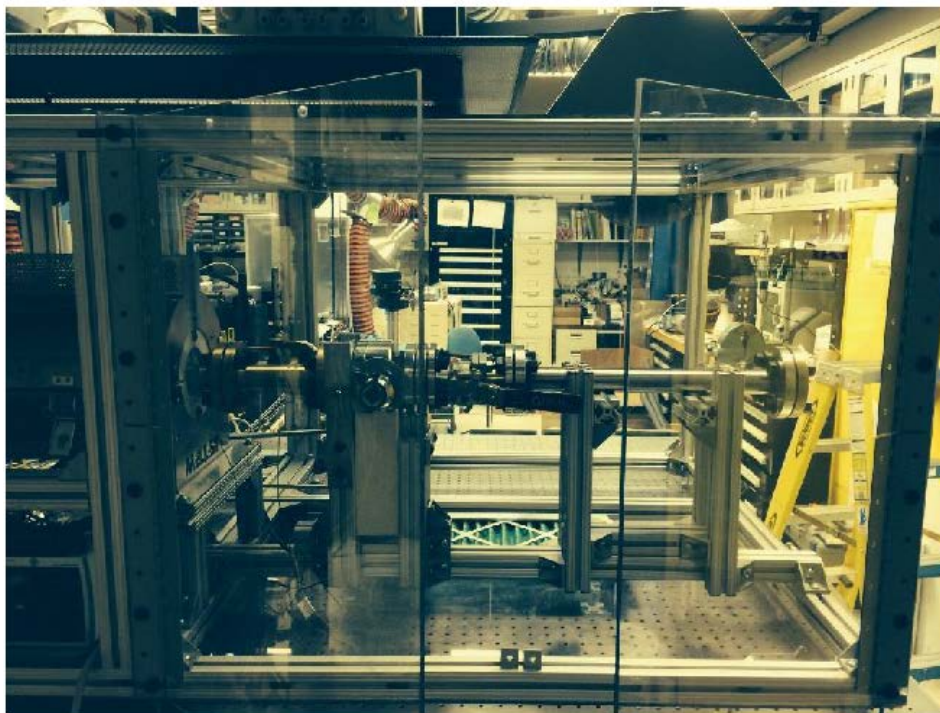
Figure 37.—CMCC EDU Reactor Assembly Outlet Gas Side.

3.2.1   Carbon Monoxide Catalytic Conversion EDU—Major Components

3.2.1.1   Furnace

The furnace within the EDU was used to heat the reactor chamber up to the test temperature, which was typically 500 °C. The furnace was a "clam shell" type furnace. The upper half of the furnace opened so that the reactor chamber could be positioned within the furnace. Figure 38 shows the furnace with the top half of the furnace closed. Figure 39 shows the furnace with the top half opened and showing the reactor chamber positioned inside the furnace.

Figure 38.—CMCC EDU Furnace and Data Acquisition System.

Figure 39.—Furnace Open Showing Reactor Assembly.

3.2.1.2   Furnace Controller and Data Acquisition System

The power to the furnace and the furnace temperature was controlled by the furnace controller shown in Figure 40. The data acquisition, also shown in Figure 40, recorded the temperatures and pressures of the sensors within the EDU. The data acquisition system was capable of recording data on up to 20 channels. A graphical display shows a time plot the sensor values, and updates the plot every 5 sec. The data was recorded on a portable flash drive that plugged into the data acquisition system.

3.2.1.3   Recuperative Heat Exchanger

A recuperative heat exchanger was connected to the reactor assembly. This heat exchanger consisted of a coiled copper tube-in-tube assembly which was placed inside a metal can and packed with insulation. As the hot gases left the reactor assembly their heat energy was transferred to the in-coming gases. The "hot-side" of the heat exchanger was connected to the reactor assembly. The hot outlet gases coming from the reactor assembly traveled through the heat exchanger's inner tube while the in-coming gases traveled through the heat exchangers shell tube that contained the inner tube. Figure 41 shows the heat exchanger prior to the insulations being added and the lid for the heat exchanger being attached. Figure 42 shows the fully assembled heat exchanger within the EDU.

Figure 40.—Furnace Controller and Data Acquisition System.

Figure 41.—Recuperative Heat Exchanger Inside.
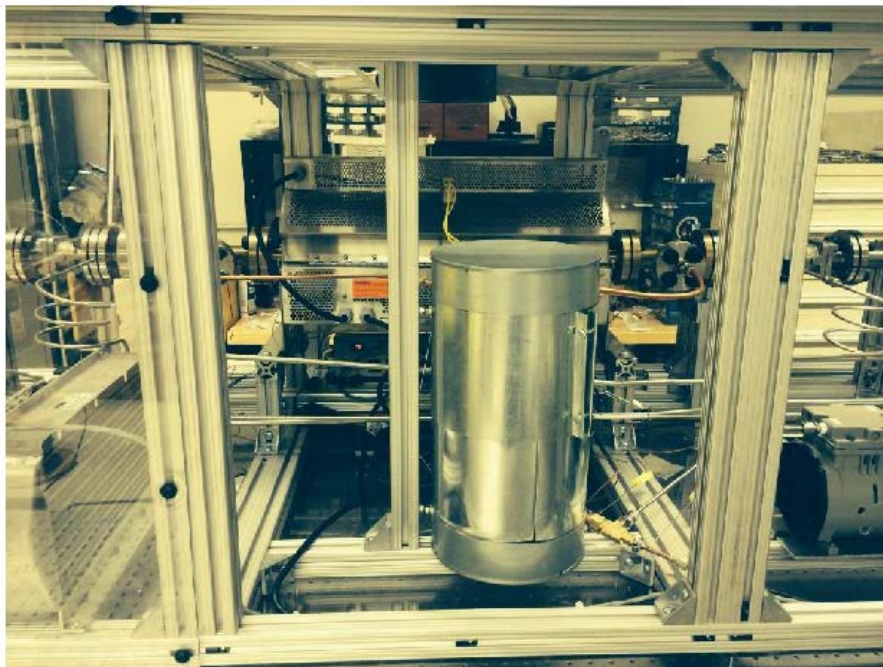
Figure 42.—CMCC EDU Showing Recuperative Heat Exchanger.

3.2.1.4 Reactor Assembly

The reactor assembly consisted of the reactor chamber, the tee sections on either end of the reactor chamber, a ball valve at each end, a servicing assembly, and a carbon/catalyst receiving assembly. Figure 43 is an illustration of the basic operation of the reactor assembly. While operating, the carbon monoxide entered the reactor assembly through the side arm of one of the tee sections. As the carbon monoxide flowed through the reactor chamber, the carbon monoxide was converted to carbon, which was retained within the reactor chamber and carbon dioxide exited the reactor assembly through the side arm of the other tee section at the opposite end from where the reactant entered. The ball valves at either end of the reactor assembly sealed the reactor chamber during this part of reactor assembly operations. Once the carbon had built up to a level that requires removal from the reactor chamber, the servicing assembly was attached. A ram which was attached to a series of straight rods, was inserted into the servicing assembly. After evacuating the gaseous contents of the reactor assembly, the ball valves at either end of the reactor assembly were opened, and the ram pushed the carbon/catalyst material out of the reactor chamber and into a tubular receiving assembly. New catalyst material was loaded in a similar manner, except that the ram was used to position the catalyst in the central portion of the tube furnace.
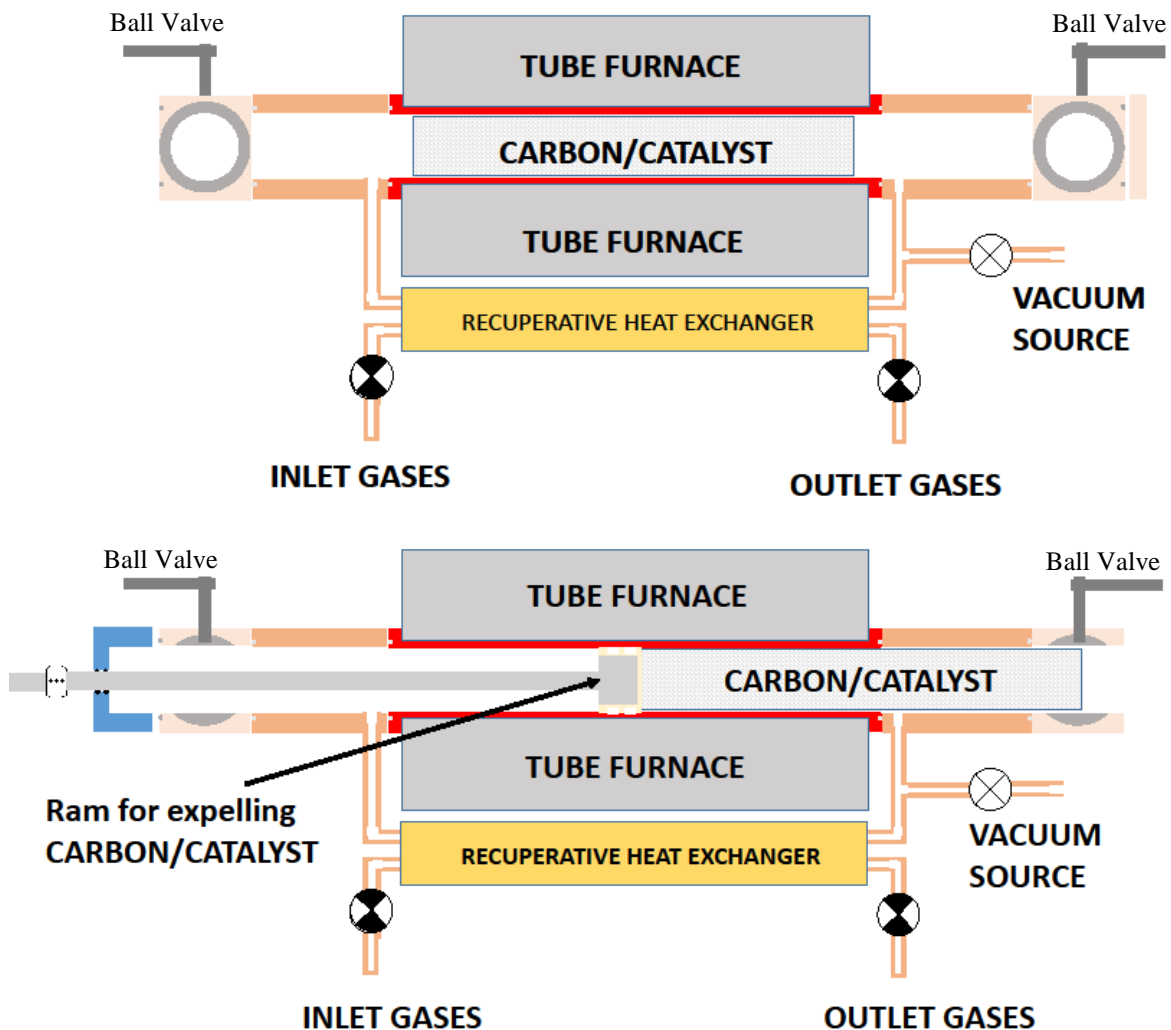
Figure 43.—Basic Operation of the Reactor Assembly.

Figure 44 shows an illustration of the Reactor Assembly (without the servicing and receiving assemblies attached). The reactor chamber and the tee sections were fabricated from Aluminum Bronze 614 which was identified by a prior development work on a Bosch reactor (Ref. 7) as being chemically compatible. Figure 45 shows the assembled reactor assembly, (including the servicing and receiving tubular assemblies), prior to being shipped to the Marshall Spaceflight Center.
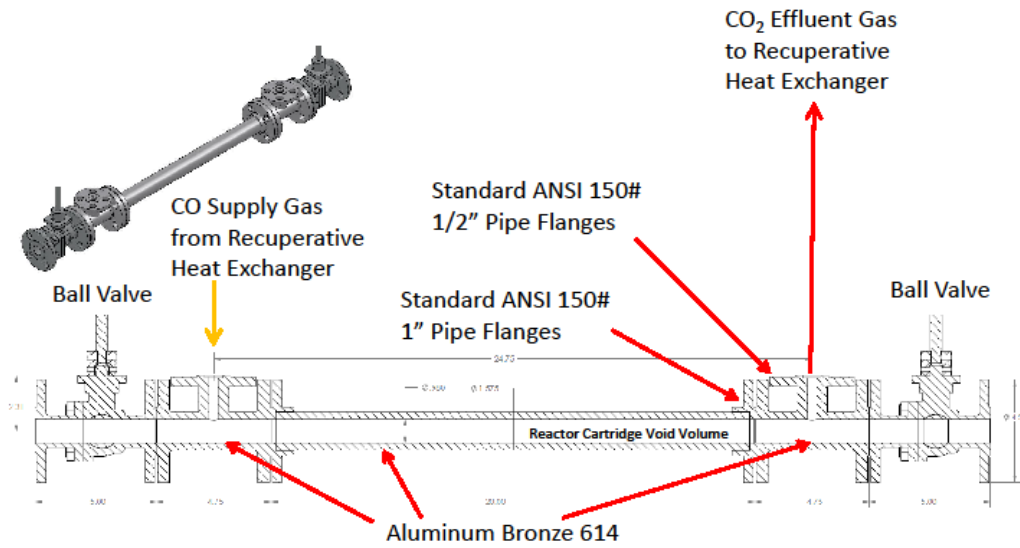
Figure 44.—Reactor Assembly.

Figure 45.—Reactor Assembly Prior to Shipment to MSFC.

3.2.1.4.1   Reactor Chamber

Figure 46 shows the Reactor Chamber. The Reactor Chamber was fabricated from Aluminum Bronze 614. It was placed in the furnace with equal lengths protruding from the sides of the furnace. The chamber had a bore of approximately one inch diameter through the entire length. The flanges on either end were 150 class ANSI flanges, but had the sealing surfaces polished to a 16 micro-inch Ra surface finish to allow the metal seals to properly seal.

3.2.1.4.2   Inlet/Outlet Tee Sections

Figure 47 shows the side and end views of one of the tee sections. The Tee sections were fabricated from Aluminum Bronze 614. One of the tee sections was connected each end of the Reactor Chamber. A metal seal was placed in the seal gland of each of the three arms of the tee. The side arm of the tees allowed the reactant gases to enter or exit the reactor chamber.

Figure 46.—Carbon Monoxide Reactor Chamber.

Figure 47.—Reactor Assembly Tee Section Side and End Views.

3.2.1.4.3   Receiver/Servicer Sections

Figure 48 shows the side and end views of Receiver/Servicer Sections. Both the Receiver Section and the Servicer Section had identical geometries and were made of 316 stainless steel. Seal glands were cut into the flanges at either end of these sections to contain the metal seals. The Receiver Section was connected to the outlet side of one of the ball valves on the outlet side of the Reactor Assembly. The Receiver Section was used to contain the carbon/catalyst material after it was expelled from the Reactor Chamber. The Servicer Section was connected to the inlet side of one of the ball valves on the inlet side of the reactor Assembly.

3.2.1.4.4   Servicer Shaft Parts

Figure 49 shows the end view of the Servicer Shaft Flange. The flange was made of 316 stainless steel. This half inch bore through this flange contained two radial seals that sealed against the push rods that were pushed through the flange while expelling used carbon/catalyst material or when positioning new catalyst material in the furnace. The Servicer Shaft Flange was attached to the end of the Servicer tube.
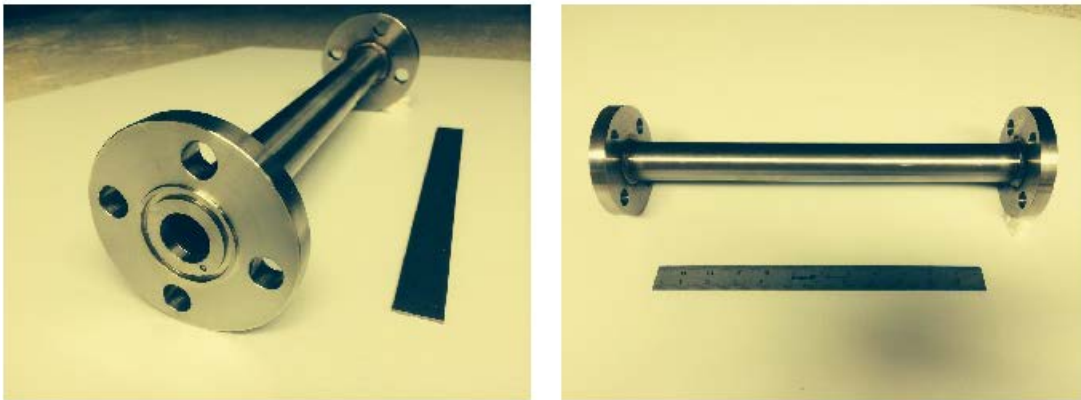
Figure 48.—Reactor Assembly Receiver/Servicer Side and End Views.

Figure 49.—Reactor Assembly Servicer Shaft Seal Section.

Figure 50 shows the push rod sections that were threaded together to produce a single rod capable of expelling the carbon/catalyst material from the furnace or positioning new catalyst material in the furnace. The rods were made of 316 stainless steel. At one end of the push rod was a ram head whose function was to sweep the inside of the reactor assembly bore and push material within the reactor assembly. The ram head was assembled from six refractory ceramic felt disks. Three of the disks had an outside diameter of slightly greater than 1 in. and three disks had a diameter of slightly less than 1 in. The disks were assembled together in an alternating size sequence as shown in the lower left quadrant of Figure 50. The disks were squeezed together by a pair of steel washers.

3.2.1.4.5   Ball Valves

Figure 51 shows the two different ball valves used in the Reactor Assembly. The Inconel ball valves shown on the left half of Figure 51 connected to the Tee Sections, and the stainless Steel ball valves shown on the right half of Figure 51 were connected to the other end of the Inconel Ball valves. These valves provided the fluid isolation during all operations of the EDU. The bore diameter of both valves was approximately 1 in.
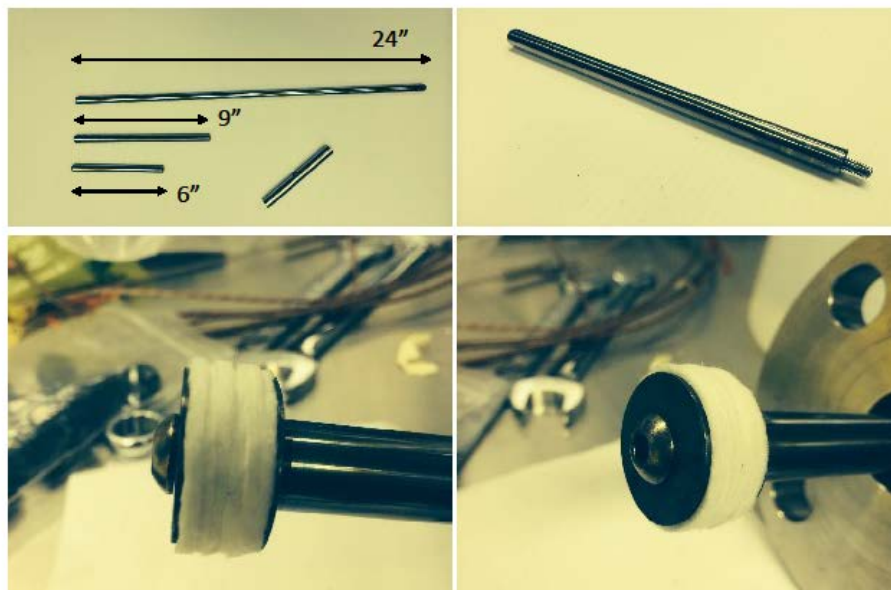
Figure 50.—Reactor Assembly Servicer Shaft Components.
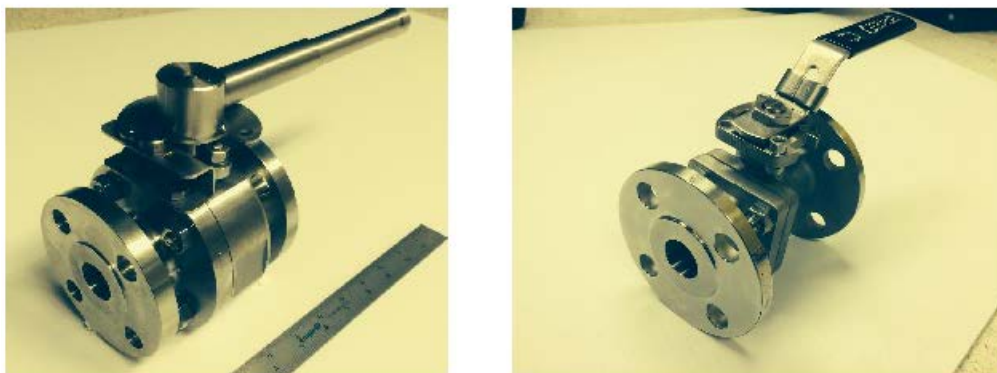
Figure 51.—Reactor Assembly High Temperature Ball Valves.

3.2.1.4.6 Metal Seals

Figure 52 shows the top and side views of the metal seals used to provide gas-tight sealing between the components of the Reactor Assembly. The seals are made from Inconel and had a very thin silver coating. The seals had a "C" cross section. As the seals are compressed between two mating parts the spring action inherent in the shape of the cross section causes the seal to press against the sealing surfaces.

Figure 53 shows a plot of the compression load versus the seal thickness for the two different size metal seals. The uncompressed thickness of the seals was approximately 0.125 in. As the load increased the seal thickness got smaller in a roughly linear fashion for both seal sizes.
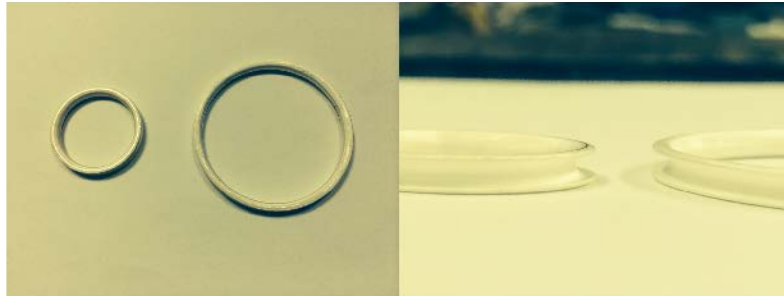
Figure 52.—Reactor Assembly High Temperature Metal Seals Top and Side Views.
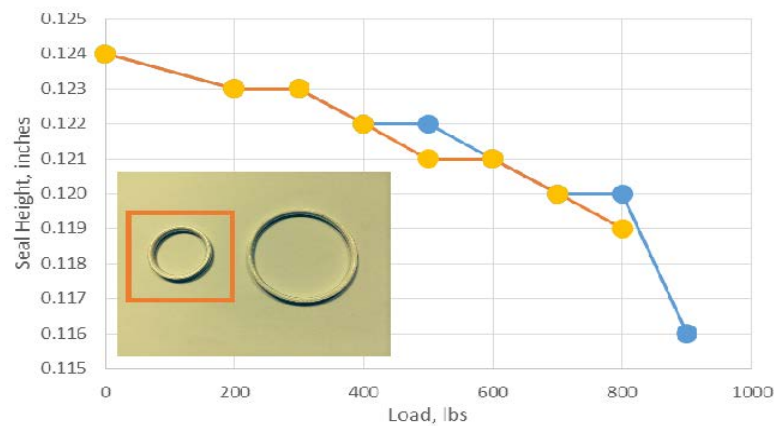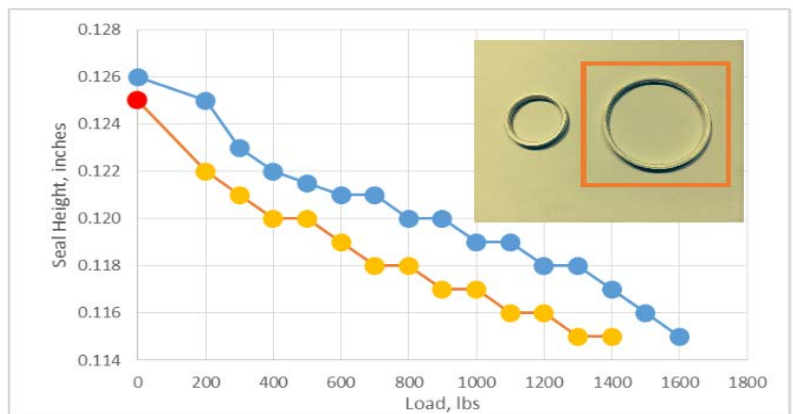
Figure 53.—Reactor Assembly High Temperature Metal Seals Compression Load.

3.2.2 CMCC EDU Testing Results

3.2.2.1 Furnace Heat-up and Cool-Down Results

Figure 54 shows the increase in temperature during heat-up of the furnace. From the initial powering of the furnace, it took about 4 to 5 hr for the furnace to stabilize in temperature. During the heat-up the furnace electrical current draw was measured with an AC amp probe. The current draw was approximately 8.7 A (approximately 1,000 W). Once the furnace temperature stabilized, the electrical current dropped and varied between 2.4 and 5.9 A (275 to 675 W). The furnace inlet and outlet temperatures were measured on the surface of the Reactor Chamber just outside the furnace enclosure. During the testing the furnace was typically left on overnight so that the running of experiments was not delayed. Figure 54 also shows the decrease in temperature during furnace cool-down. The cool-down took between 10 to 12 hr to reach ambient laboratory temperature. Because the catalyst sample materials could be unloaded from the reactor and new catalyst loaded without cooling the furnace the overall 14 to 17 hr needed for reactor cooling and re-heating was avoided, and more experiments could be run.
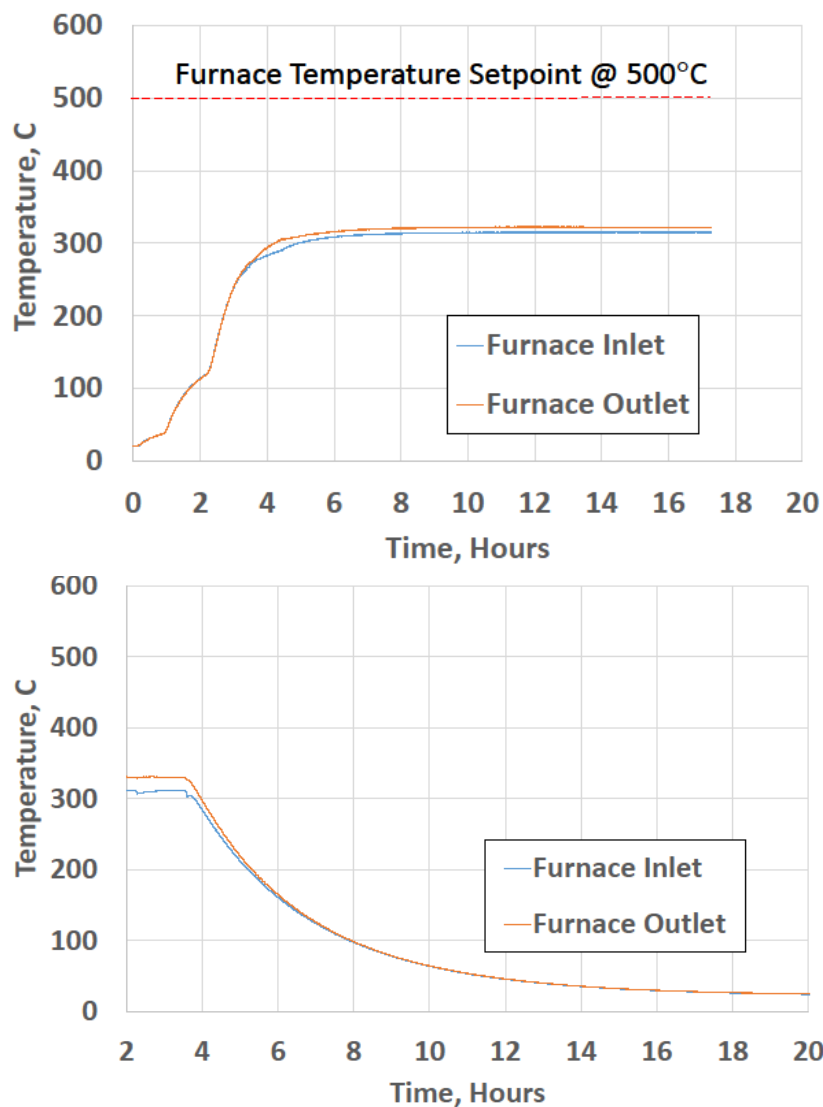
Figure 54.—Furnace Heat-Up and Cool-Down Performance.
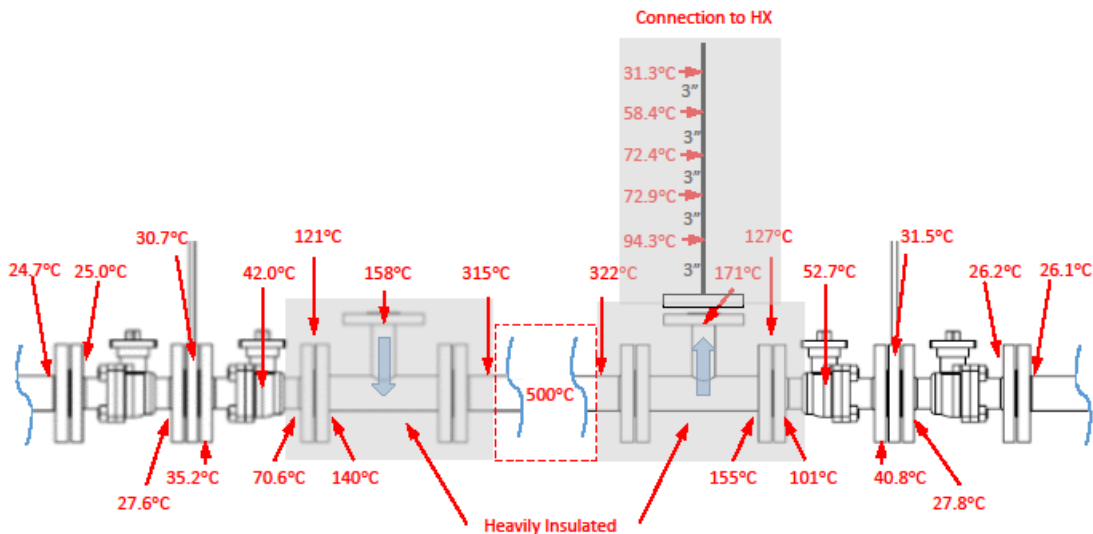
Figure 55.—Reactor Assembly Temperature Profile Outside of Furnace.

3.2.2.2　Reactor Assembly Temperature Profile Results

Figure 55 shows temperature measurements of different surface locations of the Reactor Assembly after the furnace had stabilized overnight at 500 °C. What was very noteworthy of this data was how much the temperature of the Reactor Assembly dropped once outside the furnace. Between the end of the heated zone within the furnace and the just outside the furnace enclosure was approximately 3 in., yet the temperature drop was approximately 280 °C. Despite substantial ceramic insulation, the temperature dropped another 150 to 170 °C from the point just outside the furnace to flange surfaces on the inlet and outlet Tee Sections (a distance of approximately 7 in.). The temperature dropped from 171 to 31.3 °C along the length of the tubing that connected the side-arm of the outlet Tee section to the recuperative heat exchanger, again despite heavy ceramic insulation. The result of this temperature drop was that there was almost no heat to be recovered from the hot gases leaving the Reactor Assembly to heat incoming reactants.

3.2.2.3　CMCC EDU Loading and Unloading Operation Trial Results

Prior to starting any CO conversion testing, the basic loading and unloading performance of the Reactor Assembly was tested. Because the temperature of both the Servicer tube and the Receiver tube were near ambient laboratory temperature, neither the Servicer nor Receiver tubes were disconnected from the Reactor Assembly.

The trials consisted of "dress rehearsals" of the loading and unloading procedure to work out any procedural problems as well as to evaluate the operation of the push rods and ram while the furnace was at its normal operating temperature of 500 °C. Two trials were done where the ram head was connected to the push rods and inserted into the Servicer tube. The inlet stainless steel and Inconel ball valves were opened, and the ram head was pushed through the Reactor Assembly to a point representing the center of the furnace. In both trials the ram head easily slid through the Reactor Assembly to a point representing the center of the furnace and then was withdrawn fully. A third trial was performed to simulate the removal of catalyst material from the furnace. For this trial the ram head was connected to the push rods and inserted into the Servicer tube. The inlet and outlet stainless steel and Inconel ball valves were opened, and the ram head was pushed through the Reactor Assembly to a point representing the full travel of the ram head into the receiver tube. In this trial the ram head easily slid through the Reactor Assembly and then was withdrawn fully. A fourth trial was done to repeat the earlier loading and unloading trials, but this included representative steel wool material. This trial, as with the earlier trials, the ram head slid easily through the Reactor Assembly and was withdrawn fully. In all but two tests of the EDU, the ram

head was successful in unloading spent catalyst material and positioning new catalyst material in the furnace, requiring only a few minutes to either load or unload material from the furnace while the furnace was at its normal operating temperature. In the two unsuccessful instances, the carbon had built up to a level that prevented the ram from pushing the material out of the furnace. The material was successfully removed with the aid of a small auger after the furnace had cooled down to room temperature.

3.2.2.4   CMCC EDU Catalyst Material Testing Results

This testing was to evaluate different grades of steel wool from two different manufacturers. Steel wool samples from GMT and Rhodes were tested. Grades 0, 00, 000, and 0000 of steel wool were tested. Table 3 describes the different steel wool grades.

The initial results of this testing showed inconsistent performance, even when using the same grade from the same manufacturer. A pre-treatment of the steel wool samples was done to eliminate anti-rust treatments that were on the steel wool products to prevent rust formation while on store shelves. The pretreatment of the steel wool was done by dipping the steel wool in 10 vol% acetic acid solution for 3 min followed by rinsing with deionized water and air drying. The pre-treated samples showed varying degrees of rust formation. Figure 56 shows two samples where half of the sample was treated while the other half remained untreated. These samples were positioned in the center of the Reactor Chamber and supplied a mixture of carbon monoxide and hydrogen. The effect of this pre-treatment on the catalytic performance can be seen in Figure 56. Figure 56 also shows that the effect is the same whether the sample is oriented within the furnace with the treated half on the upstream side or the downstream side. Subsequent testing was done with steel wool samples that had been treated. The comparison of manufacturers showed a slight advantage to the GMT brand over the Rhodes brand, but more significantly was that as the grade was changed to finer grades the catalytic activity became less to the point that Grades 000 and 0000 for either manufacturer were essentially not catalytic at all. All subsequent testing was done with the GMT grade 0 steel wool.

Another observation from this testing was that the formation of carbon on the samples was more concentrated at the upstream side of the sample with gradually less carbon formation at the trailing end of the sample as shown in Figure 57. A section of the sample that was most heavily carbonized was removed, measured and weighed to obtain a density. Table 4 shows the characteristics of these sections. The densities of these sections varied between 0.325 and 0.419. These values are comparable to what was achieved by General Dynamics 0.2 to 0.4 g/cm^3 (Ref. 7) and Life Systems 0.55 g/cm^3 (Ref. 8) for Bosch reactors using expendable catalysts.

TABLE 3.—CHARACTERISTICS OF STEEL WOOL GRADES

Typical Steel Wool Fiber Width								
Grade	0000	000	00	0	1	2	3	4
Name	Finest	Extra Fine	Fine	Medium Fine	Medium	Medium Coarse	Coarse	Extra Coarse
Inches	0.001	0.0015	0.0018	0.002	0.0025	0.003	0.0035	0.0047
MM	0.03	0.04	0.04	0.05	0.06	0.08	0.09	0.1
Microns	25	35	40	50	60	75	90	100

Steel Wool Catalysts Sample Upstream End Treated with 10% Acetic Acid

Steel Wool Catalysts Sample Downstream End Treated with 10% Acetic Acid
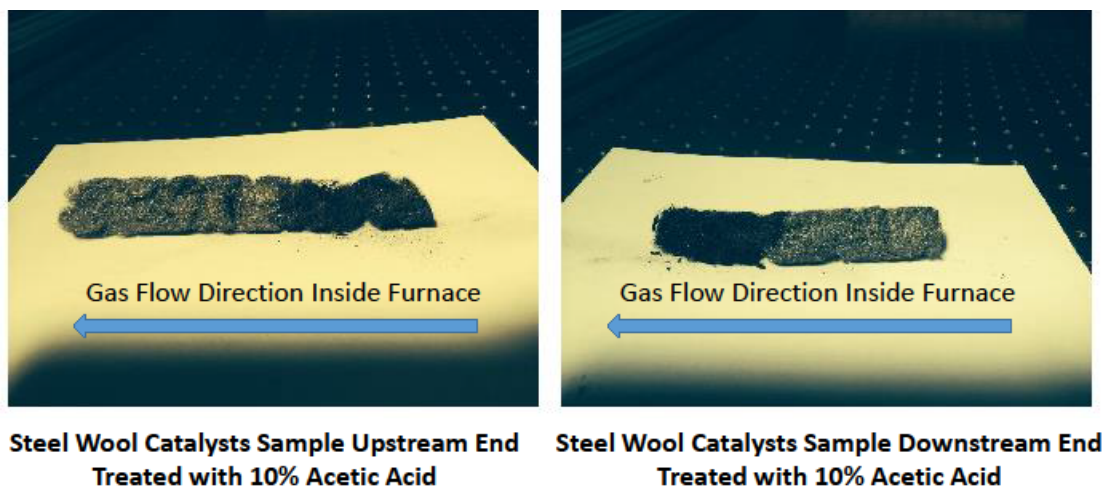
Figure 56.—Effect of Pre-Treatment on Catalyst Performance.

Figure 57.—Distribution of Carbon on EDU Catalyst Sample.

TABLE 4.—CATALYST MAXIMUM CARBONIZATION SECTION CARBON DENSITY

Sample Density Data							
Sample No.	Description	Length, in	Diameter, in	Volume, cu-in	Volume, cu-cm	Mass, g	Density, g/cu-cm
1	Heavily carbonized, but still "spongy"	1.7685	1.02	1.445	23.676	7.699	0.325
2	Very heavily carbonized, close to solid powdery "cake"	2.3145	0.9965	1.804	29.5747	12.396	0.419

3.2.2.5   CMCC EDU CO Conversion Rate Testing Results

This testing evaluated the carbon dioxide outlet concentration for three different flow rates. The outlet carbon dioxide concentration can be converted mathematically to the single pass conversion rate of carbon monoxide to carbon dioxide. Figure 58 shows the results of this testing. For each of the three experiments, the gas mixture that was fed to the reactor was 95 percent carbon monoxide and 5 percent hydrogen. The 0.355 slpm CO flow was mixed with 0.02 slpm H_2, the 0.710 slpm CO flow was mixed with 0.04 slpm H_2 and the 1.065 slpm CO was mixed with 0.060 slpm H_2. The data curves for the 0.355 and 0.710 slpm CO flows show a rapid rise in the concentration of CO_2 in the outlet stream to about 60 to 70 percent over the first 30 min, followed by a more gradual rise to about 80 percent. The conversion of this data to single pass CO conversion shows the single pass conversion rising rapidly to about 80 to 85 percent, and gradually increasing to 90+ percent. The same data for the 1.065 slpm CO flow shows a more gradual rise over about 30 min.

The catalyst mass for each of the three tests was approximately the same for each test (5 grams). Figure 59 plots the same data as in Figure 58, but the carbon deposition rate (in units of grams carbon per gram of catalyst per hour) was calculated. The rate for each test substantially exceeds the key performance parameter for the deposition rate (threshold level ≥ 0.2 grams carbon/gram catalyst/Hr; goal level ≥ 0.4 grams carbon/gram catalyst/Hr).

A gas mixture of 60%CO/20%H_2/20%CO_2 was used in a different test. The results of this test are shown in Figure 60. The outlet CO_2 concentration is about 60 percent which is similar to the tests done where the CO inlet concentration was 95 percent, but the single pass CO conversion rate was 40 percent which is less than the previous tests.

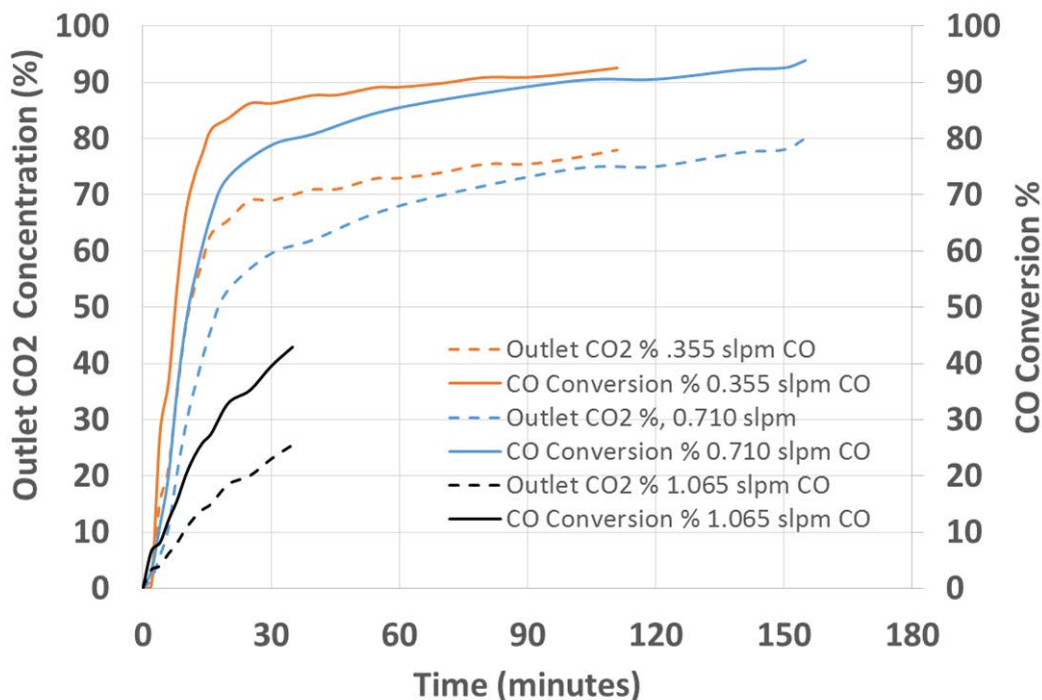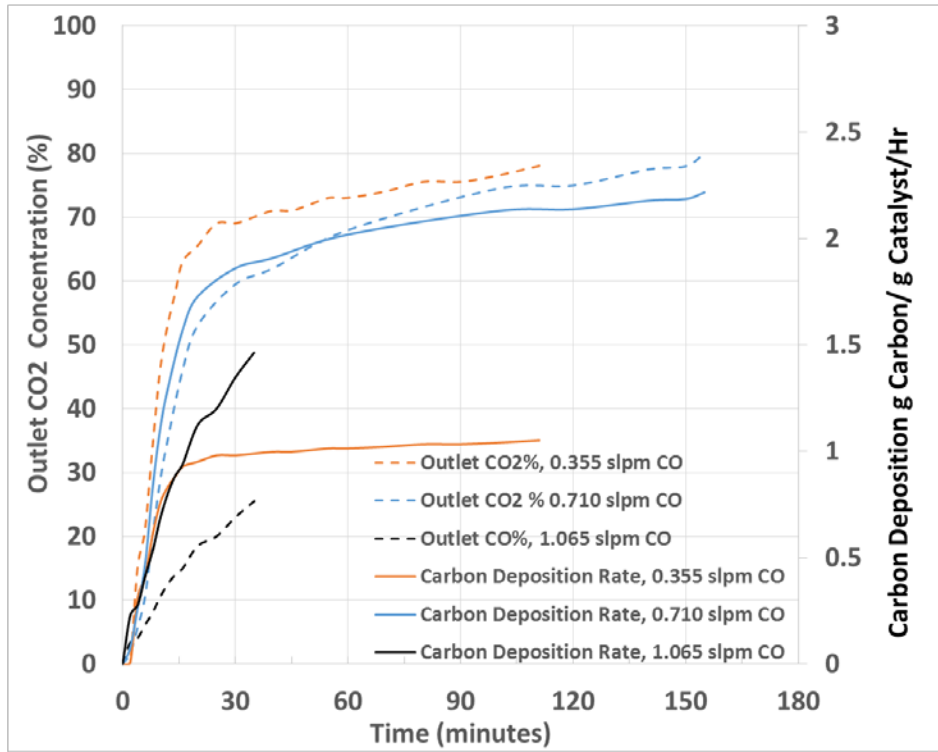Figure 58.—Outlet CO_2 Concentration and CO Conversion versus Flow Rate.

Figure 59.—Outlet CO$_2$ Concentration and Carbon Deposition Rate versus Flow Rate.
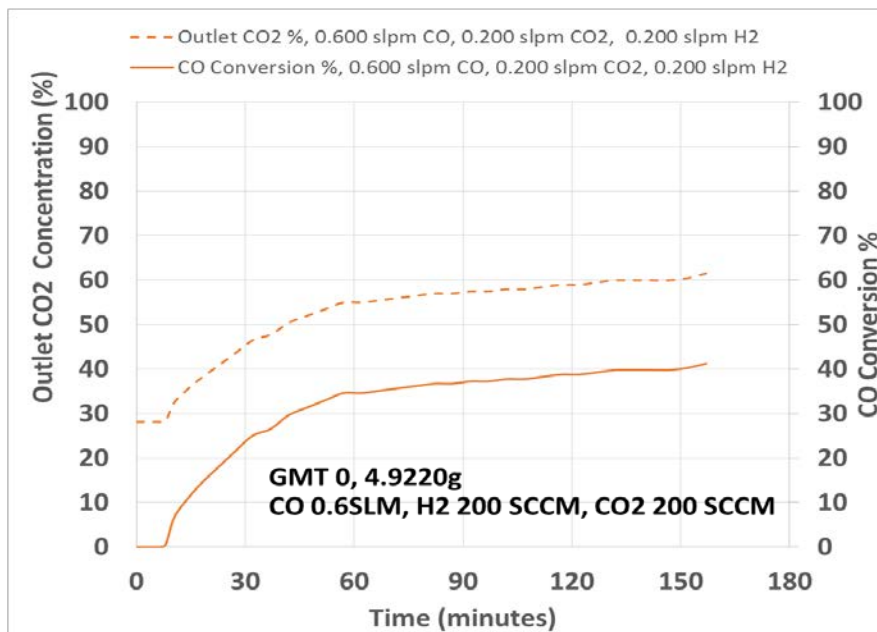

Figure 60.—Outlet CO$_2$ Concentration and CO Conversion 60%CO/20%H$_2$/20%CO$_2$.

Table 5 shows a listing of the longer duration tests (tests of two hours or longer). The carbon mass to catalyst mass was calculated for these tests. All seven of these tests exceeded the threshold key performance parameter of ≥ 2.0 grams of Carbon per gram of catalyst. Two of these tests exceeded the goal level of ≥ 4.0 grams of Carbon per gram of catalyst, but for both of these tests the carbonized sample could not be pushed out of the reactor. The distribution of the carbon in all of these tests was as illustrated in Figure 57 where the upstream section of the sample was most heavily carbonized. If the distribution of carbon were more uniform the ratios of carbon to catalyst would likely be higher.

TABLE 5.—CATALYST MAXIMUM CARBONIZATION SECTION CARBON DENSITY

Date	Time started	Time ended	Duration	Catalyst mass	Unloaded mass	Inlet Gas composition			Carbon mass	Carbon to catalyst
dd/mm/yy	hr:mm	hr:mm	minutes	grams	grams	CO%	H2%	CO$_2$%	grams	grams/gram
06/29/16	10:43	12:44	121	5.0114	17.9931	95	5	0	12.9817	2.59
06/30/16	13:39	16:39	180	5.6282	22.1732	95	5	0	16.545	2.94
07/06/16	9:49	13:49	240	5.6575	31.2667	95	5	0	25.6092	4.53
07/07/16	12:24	15:24	180	3.9954	22.794	95	5	0	18.7986	4.71
07/11/16	10:59	13:34	155	4.8308	21.0664	95	5	0	16.2356	3.36
07/11/16	15:06	17:14	128	5.0968	15.7039	80	20	0	10.6071	2.08
07/12/16	14:18	16:55	157	4.922	18.2912	60	20	20	13.3692	2.72

4.0   Summary and Conclusions

4.1   Summary

The Phase I project developed two Engineering Development Units (EDU) which were low fidelity system breadboards. Both EDUs were successfully developed and demonstrated the critical functions and basic functionality for each process. The Key performance parameters identified in the Phase I Proposal were met. The carbon dioxide electrolysis EDU was delivered to the NASA Johnson Space Center and the carbon monoxide catalytic conversion EDU was delivered to the NASA Marshall Spaceflight Center.

4.1.1   Carbon Dioxide Electrolysis

The carbon dioxide electrolysis team at the University of Delaware, which was led by Dr. Feng Jiao successfully developed an integrated CO$_2$ electrolysis EDU and delivered to NASA before the contract deadline.

Tests of a single cell, a six-cell stack and the cell stacks of the electrolysis EDU all successfully converted carbon dioxide into carbon monoxide and oxygen. The key performance parameters were met:
- The single 25 cm^2 cell, the 100 cm^2 single cell, the six-cell stack and the EDU met the key performance threshold level of ≥ 80% FaradaIc current efficiency.
- The cathode overpotential for the single 25 cm^2 cell, the single 100 cm^2 cell tests, the six-cell stack and the EDU met the key performance goal level of ≤ 0.6V.
- The current density key performance parameter threshold levels of ≥ 25 mA/cm^2 was met by the single 25 cm^2 cell, the six-cell stack, and the EDU. The key performance parameter goal level of ≥ 35 mA/cm^2 was met by the single 25 cm^2 cell.

4.1.2 Carbon Monoxide Catalytic Conversion

The carbon monoxide catalytic conversion EDU was built by the NASA Glenn Research Center with Kenneth Burke as the principal investigator and overall project leader for the development of both EDUs. The carbon monoxide conversion EDU was successfully developed and delivered to the Marshall Space Flight Center.

Tests of the catalyst samples as well as the EDU successfully converted carbon monoxide into carbon and carbon dioxide. The key performance parameters were met:

- The catalyst samples and the EDU both met the threshold level ≥ 2 gm C/gm Catalyst. The catalyst samples also met the goal level of ≥ 4 gm C/gm Catalyst.
- The catalyst samples and the EDU both met the threshold level ≥ 0.2 gm C/gm Catalyst/hr and the goal level of ≥ 4 gm C/gm Catalyst/hr.
- The catalyst samples and the EDU both met the threshold level ≤ 600 °C operating temperature.

4.2 Conclusions

The objective of the Phase I program as stated in the Task Agreement was:

"Phase I is the Engineering Development Unit (EDU) Phase, involving the design, fabrication, and demonstration of an engineering development unit (at least technology readiness level [TRL] 4) capable of empirically demonstrating the capability of the proposed technology".

NASA Procedural requirements NPR 7123.1B describes the TRL level 4 hardware as:

"A low fidelity system/component breadboard is built and operated to demonstrate basic functionality and critical test environments, and associated performance predictions are defined relative to final operating environment".

The phase I project successfully demonstrated a CO2 Electrolysis Engineering Development Unit and a Carbon Monoxide Catalytic Conversion Engineering Development Unit. Both of these units demonstrated the basic functionality and produced the test data that show that the key performance predictions identified in the Phase I proposal were met.

4.2.1 Carbon Dioxide Electrolysis

In addition to the conclusions that basic functionality and the key performance parameters were met, the following other conclusions were drawn during the course of Phase I:

- Improvements can be made in the cell/stack design by replacing PTFE with a less pliable frame material. By doing this, the force produced by the endplates can be more uniformly applied to the sealing and active areas which should reduce the probability of gas/liquid leakage out of the cell/stack and improve the electrical contact through the cell/stack.
- Improvements can be made in the cell/stack design by replacing the "square peg" supporting structure in the metal electrode plates with a different structure that provides more uniform support to the cell ion exchange membrane. By doing this, the ion exchange membrane will be less prone to puncture. Also the electrical contact and electrochemical performance will be improved.
- Improvements can be made in the cell/stack design by replacing the silicone gaskets with a sealing O-ring. By doing this, the probability of gas/liquid leakage out of the cell/stack will be reduced.
- Replacing the sodium ion in the circulating catholyte with a different ion could improve the performance stability by reducing the exchange of catholyte positive ions with the H^+ ions in the ion exchange membrane.

- The CO Faradaic efficiency of the EDU could be further improved by increasing the electrolyte flow rate and the electrolyzer operation pressure.

4.2.2 Carbon Monoxide Catalytic Conversion

In addition to the conclusions that basic functionality and the key performance parameters were met, the following other conclusions were drawn during the course of Phase I:

- The basic operation approach to operating the carbon formation reactor that allows the carbon to be removed and catalyst replaced while keeping the reactor at its operating temperature is very workable and offers substantial system benefits of quick and energy efficient carbon removal/catalyst replacement.
- Optimization of the structure of the catalyst load in the reactor can improve the efficient and uniform use of catalyst that will increase the mass of carbon deposited per unit mass of catalyst. This will also prolong the length of time between catalyst loadings.
- Pre-treatment of the catalyst to remove anti-oxidation agents is essential to effective operation. Finer grades of steel wool which were not catalytic, even after the pre-treatment could be made catalytic if the appropriate pre-treatment is used. Finer grades of steel wool, with higher surface area per mass of steel would be expected to be more effective catalysts.
- Recovering the heat from the exit gases to pre-heat the incoming gases can be done, but the amount of heat recovered versus the mass and volume of the recuperating heat exchanger is not a good trade from a system level. Future designs without the recuperating heat exchanger will be substantially smaller and lighter and with acceptable losses in energy recovery.
- The temperature profile outside of the heated part of the reactor falls off substantially in temperature over short distances outside the reactor despite heavy insulation around the inlet and exit piping. This has the beneficial effect of reducing the heat resistance required of components immediately outside of the reactor. Metal seals in some instances can be replaced with elastomer O-rings that provide more forgiving sealing.
- The aluminum bronze material used for the reactor was very satisfactory. The use of an alumina ceramic is unnecessary. Also vendors to fabricate the aluminum bronze are more readily available. Since the aluminum bronze is much tougher than ceramic, the reactor design is much less susceptible to fracture, and parts can be made with thinner cross sections. This would result in lighter and stronger reactors with no loss in long term chemical stability. Also the reactor assembly can be made from fewer pieces that are welded together which reduces mass and improves leak-tightness.
- The high single pass conversion of carbon monoxide means that there is no need to recycle the gases within the carbon formation reactor. This results in an overall simpler design.

5.0   Recommendations for Phase II

The recommendations for Phase II fall generally into four different categories, scale-up, integration, automation, and performance enhancements/optimizations.

5.1   Scale-up

Both the carbon dioxide electrolysis process and the carbon monoxide catalytic conversion were implemented at a scale that is below the four-person level needed for deeper space manned exploration. Both processes need to be scaled up to a four person performance size.

For the electrolysis process this will require larger electrodes or operating the smaller electrodes at higher current densities, or both. The larger 100 cm^2 electrodes tested in Phase I will need to be assembled into multicell stacks. If the operating current density can be substantially increased the number of cells/stacks could be reduced.

For the carbon monoxide catalytic conversion process, the scale up will require increasing the diameter if the reactor from the 1 in. diameter in Phase I to a 5 or 6 in. diameter in Phase II. The increase in diameter has a substantial impact on the other reactor assembly components, so the scale-up of the valves, servicer, and receiver sections will be important to address.

5.2   Integration

Phase II will require the integration of the two processes. The means to match the rate of chemical processing of each process will need to be addressed since a mismatch in the rates will result in an accumulation of reactant in the slower rate process. This will be essential because the conversion of carbon monoxide will go through periods of inactivity because the carbon is being removed, Integration will also require producing a carbon particulate-free recycle flow from the carbon formation reactor to the carbon dioxide electrolyzer by filtering the carbon particulates from the recycle flow. Integration will also require the elimination of hydrogen from the system. Hydrogen is produced by the electrolyzer in quantities great enough that if not eliminated from the system, will build up to concentrations that will impede both processes. Suitable solutions to each of these integration issues will need to be developed and tested prior to integration early to minimize the integration risk.

5.3   Automation

Automation of each process as well as the integrated assembly of the two processes will be required for Phase II. Minimizing operator intervention by automation will be needed to prevent excessive use of astronaut's time as well as to provide quick and effective action should a problem develop. The control aspects of automation will be important to manage for what may be a time-varying need to process carbon dioxide into carbon and oxygen. The manual nature of the carbon monoxide conversion EDU will need to be a more automated process of loading and unloading material in the reactor.

5.4   Performance Enhancements/Improvements

Listed in sections 4.2.1 and 4.2.2 are improvements and enhancements to what was developed in Phase I. Some of what is listed in these two sections are straight-forward and low risk to implement, while others may involve greater time to investigate and implement. While enhancements and improvements are desirable, the accomplishment of these improved features are not as important to the end objective of Phase II as the other recommended areas, so the implementation of these enhancements and improvements should not be accomplished at the expense of the other essential areas.

Appendix A.—CMCC EDU P&ID and Electrical Schematics

CMCC EDU P & ID

CMCC EDU Electrical Schematic

Appendix B.—List of Abbreviations, Acronym, and Symbols

Abbreviations and Acronyms

ANSI	American National Standards Institute
CMCC	Carbon Monoxide Catalytic Conversion
ECLSS	Environmental Control Life Support System
EDS	Electron Dispersive Spectroscopy
EDU	Engineering Development Unit
DI	Deionized Water
Ir-CCM	Iridium Coated Cation Exchange Membrane
KPP	Key Performance Parameter
MSFC	Marshall Spaceflight Center
NASA	National Aeronautics and Space Administration
P&ID	Process and Instrumentation Diagram
PTFE	Polytetrafluoroethylene
RHE	Reversible Hydrogen Electrode
SEM	Scanning Electron Microscope

Symbols

A	Ampere	Hr	Hour
AC	Alternating Current	Ir	Iridium
Ag	Silver	m	Meter
Al	Aluminum	mA	Milli-Amp
°C	Degree Celsius	min	Minute
C	Carbon	mL	Milliliter
CO	Carbon Monoxide	O_2	Oxygen
CO_2	Carbon Dioxide	OH^-	Hydroxyl Ion
cm	Centimeter	Pt	Platinum
e^-	Electron	psi	Pounds per Square Inch
H_2	Hydrogen	V	Volt
H_2O	Water	Vol%	Percent Volume
H^+	Proton	wt%	Percent Weight
HCl	Hydrochloric Acid		

References

1. Feng Jiao, et al, Nature Communications "A Selective and Efficient Electrocatalyst for Carbon Dioxide Reduction," 30 January 2014.
2. Delaware Metal, 400 Water Street, Newport, Delaware19804.
3. Hunt, J., Ferrari, A., Lita, A., Crosswhite, M., Ashley, B., & Stiegman, A.E. (2013). Microwave-specific enhancement of the carbon-carbon dioxide (Boudouard) reaction. The Journal of Physical Chemistry C, 117 (51) 26871-26880.
4. Gonzalez-Blanco, O.J. & Branchadell, V. (1999). Density functional study of the Fe-CO bond dissociation energies of Fe(CO)5. Journal of Chemical Physics, 110(2), 778–783.
5. Sunderlin, L.S., Dingneng, W., & Squires, R.R. (1993). Bond strengths in first-row-metal carbonyl anions. Journal of the American Chemical Society, 115(25), 12060–12070.
6. Sunderlin, L.S., Dingneng, W., & Squires, R.R. (1992). Metal (iron and nickel) carbonyl bond strengths in Fe(CO)n- and Ni(CO)n-. Journal of the American Chemical Society, 114(8), 2788–2796.
7. Holmes, R.F., King, C.D., Keller, E.E. General Dynamics Convair Division, Bosch CO_2 Reduction System Development, Final Report April 1976, NASA Contract NAS8-27276.
8. Heppner, D.B., Wynveen, R.A., Schubert, F.H., Life Systems, Preprototype Bosch CO_2 Reduction Subsystem for RLSE Experiment, Final Report December 1977, NASA Contract NAS8-32492.
9. Abney, Morgan B., Mansell, J. Matthew, NASA Marshall Spaceflight Center, Evaluation of Bosch-Based Systems Using Non-Traditional Catalysts at Reduced Temperatures, July 17, 2011.